Article

Cell Reports

Paired Related Homeobox Protein 1 Regulates Quiescence in Human Oligodendrocyte Progenitors

Graphical Abstract

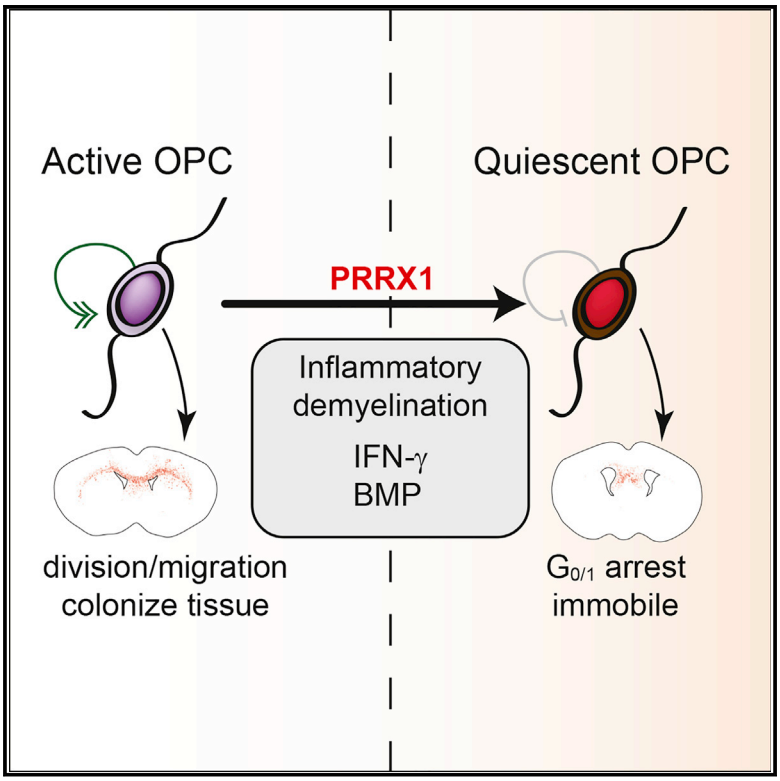

Authors

Jing Wang, Darpan Saraswat, Anjali K. Sinha, ..., Suyog U. Pol, Hani J. Shayya, Fraser J. Sim

Correspondence

fjsim@buffalo.edu

In Brief

Wang et al. investigate the role of transcription factor PRRX1 in human oligodendrocyte progenitor cells. PRRX1 induces reversible cell-cycle arrest, resulting in a quiescent-like state that prevents colonization and myelination of hypomyelinated *shiverer* mice. PRRX1 expression was regulated by interferon-γ and BMP and required for interferon-induced quiescence.

Highlights

- Transcription factor PRRX1 is expressed by quiescent human OPCs (hOPCs)
- PRRX1a induces hOPC cell-cycle arrest and inhibits migration *in vitro* and *in vivo*
- PRRX1 prevents efficient engraftment and tissue colonization by transplanted OPCs
- PRRX1 is upregulated by IFN-γ and BMP and is required for IFN-induced quiescence

Wang et al., 2018, Cell Reports *25*, 3435–3450
December 18, 2018
https://doi.org/10.1016/j.celrep.2018.11.068

CellPress

Cell Reports
Article

Paired Related Homeobox Protein 1 Regulates Quiescence in Human Oligodendrocyte Progenitors

Jing Wang,[1,4] Darpan Saraswat,[1,4] Anjali K. Sinha,[2,4] Jessie Polanco,[2] Karen Dietz,[1] Melanie A. O'Bara,[1] Suyog U. Pol,[1,3] Hani J. Shayya,[1] and Fraser J. Sim[1,2,5,*]

[1]Department of Pharmacology and Toxicology, Jacob's School of Medicine and Biomedical Sciences, University at Buffalo, Buffalo, NY, USA
[2]Neuroscience Program, Jacob's School of Medicine and Biomedical Sciences, University at Buffalo, Buffalo, NY, USA
[3]Department of Biomedical Engineering, Jacob's School of Medicine and Biomedical Sciences, University at Buffalo, Buffalo, NY, USA
[4]These authors contributed equally
[5]Lead Contact
*Correspondence: fjsim@buffalo.edu
https://doi.org/10.1016/j.celrep.2018.11.068

SUMMARY

Human oligodendrocyte progenitor cells (hOPCs) persist into adulthood as an abundant precursor population capable of division and differentiation. The transcriptional mechanisms that regulate hOPC homeostasis remain poorly defined. Herein, we identify paired related homeobox protein 1 (PRRX1) in primary PDGFαR$^+$ hOPCs. We show that enforced PRRX1 expression results in reversible $G_{1/0}$ arrest. While both PRRX1 splice variants reduce hOPC proliferation, only PRRX1a abrogates migration. hOPC engraftment into hypomyelinated *shiverer/rag2* mouse brain is severely impaired by PRRX1a, characterized by reduced cell proliferation and migration. PRRX1 induces a gene expression signature characteristic of stem cell quiescence. Both IFN-γ and BMP signaling upregulate PRRX1 and induce quiescence. PRRX1 knockdown modulates IFN-γ-induced quiescence. In mouse brain, PRRX1 mRNA was detected in non-dividing OPCs and is upregulated in OPCs following demyelination. Together, these data identify PRRX1 as a regulator of quiescence in hOPCs and as a potential regulator of pathological quiescence.

INTRODUCTION

Unlike other transient amplifying cells, oligodendrocyte progenitor cells (OPCs) persist throughout adulthood and remain a mitotic progenitor pool capable of generating new oligodendrocytes (Rivers et al., 2008; Dimou et al., 2008). Timely differentiation of these progenitors is necessary for efficient remyelination (Franklin, 2002) and motor skill learning (McKenzie et al., 2014; Marques et al., 2016). In addition to their role as a source of new oligodendrocytes, it is apparent that the function of adult OPCs is vital for normal brain function (Birey et al., 2015). OPC density is tightly regulated *in vivo*, such that loss of a single OPC, by death or differentiation, is replaced by mitosis and migration (Hughes et al., 2013). However, the molecular mechanisms that regulate OPC homeostasis in adult brain are poorly understood.

Although OPCs represent the most abundant progenitor in the adult CNS, most have been considered quiescent (Dawson et al., 2003). Fate-mapping studies indicate that likely all adult OPCs undergo cell division and that OPC cell-cycle length dramatically increases with age, from days to several months in aged animals (Psachoulia et al., 2009; Young et al., 2013). Thus, adult OPCs can enter a reversibly quiescent state for extended periods in adult brain but eventually reenter the cell cycle.

Cellular quiescence is characterized by reversible cell-cycle exit and downregulation of genes important for DNA replication, cell-cycle progression, metabolism, and protein synthesis (Rumman et al., 2015). Quiescence is essential for maintaining cell populations in reserve for tissue regeneration and repair. For example, loss of quiescence in muscle stem cells depletes the stem cell pool, leading to failed regeneration (Shea et al., 2010; Mourikis et al., 2012). Quiescent OPCs are observed in chronic demyelinated lesions in multiple sclerosis (MS) (Wolswijk, 1998). Thus, although OPCs are present in most chronic MS lesions, their number and/or density may be lower than is necessary for efficient repair (for review, see Dietz et al., 2016). As such, an additional explanation for failed remyelination could be due to pathological quiescence.

We have identified several transcription factors that were upregulated in human OPCs (hOPCs) relative to neural progenitor cells (NPCs) during lineage specification (Wang et al., 2014). Among these, paired related homeobox protein 1 (PRRX1) was implicated in adult murine NPC self-renewal (Shimozaki et al., 2013). In this study, we examined the role of PRRX1 in the regulation of hOPC function *in vitro* and following transplantation into hypomyelinated *shiverer/rag2* brain. PRRX1 overexpression led to profound and reversible arrest of the cell cycle, resulting in reduced engraftment and myelination in *shiverer* mice. We determined that PRRX1 induced a conserved gene signature involved in establishing cellular quiescence. PRRX1 was upregulated in response to known inducers of quiescence and was necessary for cell-cycle arrest.

RESULTS

PRRX1 Suppresses hOPC Proliferation and Migration *In Vitro*

Because the two PRRX1 spliced variants encode structurally distinct isoforms (Reichert et al., 2013), we sought to better

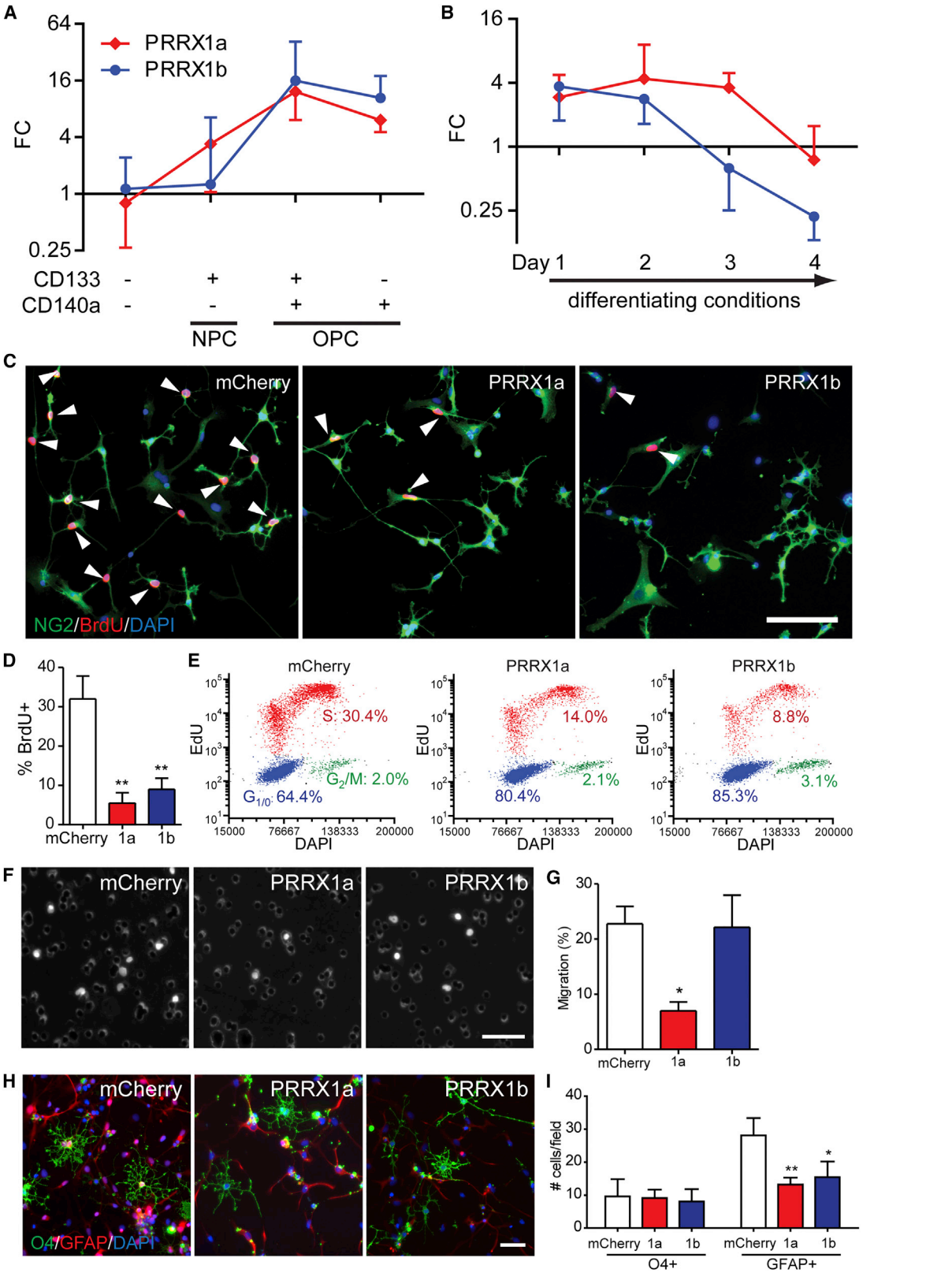

(legend on next page)

define the PRRX1 expression profile. Using CD140a/CD133 fluorescence-activated cell sorting (FACS) (Wang et al., 2013), both PRRX1a and PRRX1b mRNAs were enriched in platelet-derived growth factor (PDGF) αR^+ OPCs compared to $CD133^+$ NPCs (Figure 1A). In parallel experiments, hOPCs were induced to differentiate as immature oligodendrocytes for up to 4 days *in vitro* (Pol et al., 2017). We found that both PRRX1a and PRRX1b mRNA were downregulated as hOPCs underwent oligodendrocytic differentiation (Figure 1B). A similar pattern was found in mouse OPCs, with downregulation occurring in differentiated oligodendrocytes (Zhang et al., 2014).

In human NPCs, PRRX1 overexpression did not potentiate oligodendrocyte progenitor and oligodendrocyte generation, suggesting that it may have a role other than induction of OPC fate per se (Wang et al., 2014). As such, we investigated whether PRRX1a and PRRX1b might differentially regulate hOPC specification, migration, proliferation, and differentiation. hOPCs were infected with lentivirus (LV) encoding PRRX1a, PRRX1b, or mCherry as control. After 4 days in serum-free medium (SFM) containing PDGF AA, the percentage of proliferating (bromodeoxyuridine $[BrdU]^+NG2^+$) OPCs was significantly reduced following PRRX1a and PRRX1b overexpression compared to mCherry control cells (5.5% ± 2.6% and 9.0% ± 2.8%, respectively, versus 32.0% ± 5.8%; n = 4, $p < 0.01$, one-way repeated-measures ANOVA, Dunnett's post-test) (Figures 1C and 1D). PRRX1 substantially increased the percentage of cells in $G_{1/0}$, indicating that PRRX1 overexpression resulted in cell-cycle arrest (Figure 1E).

Next, because insufficient migration of OPCs may contribute to impaired remyelination (Boyd et al., 2013), we determined whether PRRX1 influenced migration. We measured migration in transwell-based assays following PRRX1a- or PRRX1b-expressing LV infection. hOPC migration was differentially regulated by PRRX1 variants (Figures 1F and 1G). Only 7.0% ± 1.6% of PRRX1a cells migrated toward PDGF-AA (100 ng/mL), whereas 22.8% ± 3.1% of control, mCherry-infected, and 22.2% ± 5.8% of PRRX1b-infected hOPCs migrated (n = 5 per group, $p < 0.05$, one-way repeated-measures ANOVA, Dunnett's post-test).

We next asked whether PRRX1a/b would influence hOPC fate when cultured in differentiating conditions. PRRX1 did not influence the total number of $O4^+$ oligodendrocytes; however, it reduced the $GFAP^+$ astrocyte number. Specifically, the average number of $O4^+$ cells per field did not differ (mCherry, 9.6 ± 5.2; PRRX1a, 9.1 ± 2.6; PRRX1b, 8.1 ± 3.7); however, there was a significant reduction in the $GFAP^+$ cell absolute number with PRRX1a/b overexpression (13.2 ± 2.1 and 15.5 ± 4.7, respectively, versus 28.1 ± 5.3; n = 4, $p < 0.01$, one-way repeated-measures ANOVA, Dunnett's post-test) (Figures 1H and 1I). While the absolute number of astrocytes was reduced, the proportion of $GFAP^+$ astrocytes was unaffected. The proportion of $O4^+$ oligodendrocytes was increased by PRRX1a/b (22.7 ± 2.9 and 19.8 ± 2.8, respectively, versus 13.3 ± 4.0; n = 4, $p < 0.05$, Dunnett's post-test). Consistent with a primary effect on proliferation, the total number of cells was substantially reduced with PRRX1 overexpression (live cells/field: mCherry, 72.4 ± 22.6; PRRX1a, 43.6 ± 11.5; PRRX1b, 38.0 ± 12.2; p = 0.06, one-way repeated-measures ANOVA). This decrease was not due to increased apoptosis, because equivalent rates of cleaved caspase-3 were observed (5.9% ± 0.3% and 4.1% ± 0.5%, control and PRRX1a, respectively). To exclude other forms of cell death, we assessed cell viability and death at 48 hr. PRRX1a LV had no effect on cellular morphology or live:dead ratio compared to mCherry (mCherry: 1.3 ± 0.1, PRRX1a: 1.4 ± 0.1; ratio of calcein: DAPI; n = 3 fetal samples, $p > 0.05$, t test).

A key aspect of quiescence versus senescence is the reversible nature of cell-cycle arrest. To determine whether transient PRRX1a-FLAG expression induced reversible cell-cycle arrest, we used a doxycycline-inducible LV (Figure 2). Doxycycline-induced PRRX1a significantly reduced hOPC proliferation (control, 43% ± 4%, versus doxycycline-induced PRRX1, 16% ± 4%; n = 4 fetal samples, $p < 0.01$, t test). Among $FLAG^+$ cells at 3 days, only 7.8% ± 2% were $BrdU^+$, indicating a profound effect in PRRX1-expressing hOPCs. If doxycycline was maintained for 13 days, we did not observe $BrdU^+FLAG^+$ cells, indicating that PRRX1 was sufficient to arrest proliferation. To determine whether hOPCs could reenter the cell cycle following PRRX1 downregulation, doxycycline was removed in matched cultures at day 3 (ON-OFF) (Figure 2A) and cell-cycle reentry was determined. In ON-OFF cultures, PRRX1a-FLAG expression was no longer detected, and the proportion of proliferating hOPCs had returned to control levels (OFF, 39.7% ± 3.7%, versus

Figure 1. PRRX1a/b Are Expressed by hOPCs and Differentially Regulate Proliferation, Migration, and Differentiation

(A) Human NPCs ($CD133^+CD140a^-$), early OPCs ($CD133^+CD140a^+$), and late OPCs ($CD133^-CD140a^+$) were isolated from fetal 18–22 weeks gestational age brain by FACS (n = 3 individual human samples).

(B) $PDGF\alpha R^+$ hOPCs were isolated and underwent oligodendrocyte differentiation in the absence of mitogens for up to 4 days (n = 4 human samples). qPCR was performed on RNA extracted immediately post-sort or after 1–4 days in culture. Mean ± SEM fold change (FC) shown relative to fetal dissociate ($CD133^-CD140a^-$) after GAPDH normalization.

(C–E) Fetal $PDGF\alpha R^+$ hOPCs infected with mCherry (control) or PRRX1 LV were maintained in SFM with platelet-derived growth factor (PDGF)-AA for 4 days.

(C) 24-hr BrdU incorporation was assessed in $NG2^+$ OPCs (arrowheads indicate $BrdU^+$ cells).

(D) Quantification of BrdU percentage in $NG2^+$ hOPCs (n = 4 fetal samples, $^{**}p < 0.01$ versus mCherry, one-way repeated-measures ANOVA, Dunnett's post-test).

(E) Flow cytometry of S-phase entry (red, 24-hr EdU incorporation) and $G_{1/0}$ and G_2/M phases (blue and green, respectively).

(F) LV-infected hOPC migration seeded on transwell membranes. Migrant $DAPI^+$ cells (100 ng/mL) were imaged.

(G) Percentage of migrating cells was assessed (n = 5 fetal samples, $^{*}p < 0.05$ versus mCherry, one-way repeated-measures ANOVA, Dunnett's post-test).

(H) LV-infected hOPCs were allowed to differentiate for 2 days following mitogen withdrawal in the presence of 40 ng/mL T3. Cultures were immunostained with an immature oligodendrocyte marker (O4, green) and an astrocyte marker (GFAP, red).

(I) Average number of oligodendrocyte and astrocytes in each field was quantified (n = 4 fetal samples, $^{*}p < 0.05$, $^{**}p < 0.01$ versus mCherry, one-way repeated-measures ANOVA, Dunnett's multiple comparisons post-test).

For bar charts, mean ± SEM is shown. Scale: 50 μm.

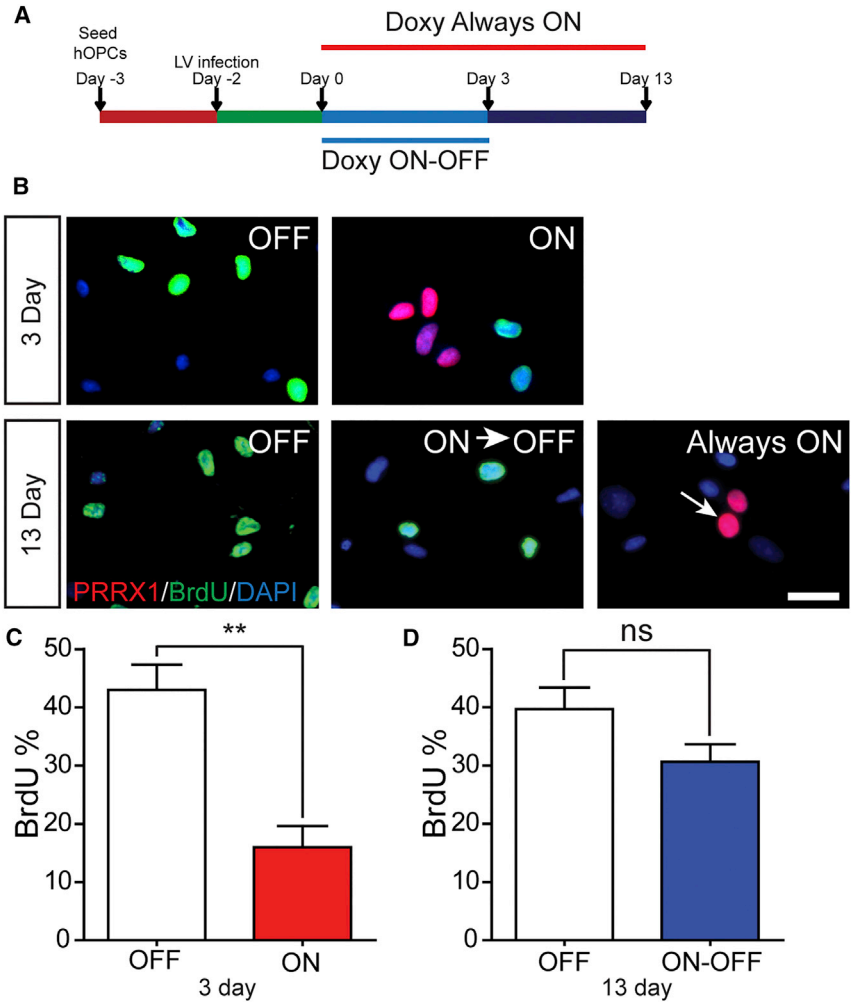

Figure 2. Transient PRRX1 Expression Results in Reversible Cell-Cycle Arrest

(A) hOPCs were infected with doxycycline-inducible FUW-PRRX1a-FLAG LV. Matched cultures were assigned to OFF (no doxycycline), ON-OFF (doxycycline for first 3 days), or Always ON (doxycycline for 13 days).

(B) hOPC proliferation was assessed by BrdU incorporation (green, 24-hr terminal pulse) at both 3 days and 13 days. PRRX1a-FLAG expression was detected by immunostaining (red).

(C and D) Quantification of BrdU at day 3 (C) and day 13 (D) (n = 3–4 fetal samples).

**p < 0.01, paired t test. For bar charts, mean ± SEM is shown. Scale: 50 μm.

ON-OFF, 30.7% ± 2.9%; n = 3, p > 0.05), representing a significant increase compared to day 3 (ON, p < 0.05). As such, these data indicate that PRRX1a can induce reversible hOPC cell-cycle arrest.

PRRX1a Overexpression Inhibits Migration of Engrafted hOPCs

To determine whether PRRX1 overexpression would induce quiescence in hOPCs *in vivo*, we transplanted LV-infected hOPCs into hypomyelinated and immunocompromised *shiverer/rag2* mice. PRRX1a/b overexpression was confirmed in engrafted cells (Figure S1). At 12 weeks, human nuclear antigen-positive (hNA$^+$) cells were largely confined to white matter (n = 4–9 per group). PRRX1a overexpression significantly impaired the rostrocaudal and lateral distribution of hOPCs compared to mCherry transplants (Figure 3A). We found that PRRX1a-infected hOPCs were distributed over a smaller region of *shiverer/rag2* forebrain (mCherry, 4.7 ± 0.1 mm; PRRX1a, 3.1 ± 0.3 mm; p < 0.01) (Figure 3B). As observed *in vitro*, PRRX1b did not affect migration after engraftment at 12 weeks. PRRX1a overexpression resulted in a substantial reduction in density and overall number of hNA$^+$ cells at 12 weeks. The callosal density of hNA$^+$ cells were reduced by >4-fold relative to mCherry-infected hOPCs (290.8 ± 75.9 versus 1,272.4 ± 316.8 cells/mm^2; p < 0.01, two-way ANOVA, Bonferroni's post-test) (Figure 3C). While the density of PRRX1b-infected cells was reduced by >25%, this was not statistically significant (952.6 ± 208.3 cells/mm^2). Immunoreactivity for cleaved caspase-3 was similarly rare among the groups at 12 weeks (data not shown), suggesting that PRRX1 overexpression did not increase cell death.

We hypothesized that the reduced cell density would be the result of impaired proliferation. Next, we determined the proportion of Ki67$^+$ cells among hNA$^+$ cells (Figures 4A and 4B). Because hOPC density is negatively correlated with proliferation (r = −0.836; p < 0.01) (Figure S2) (Windrem et al., 2008), proliferation was calculated from engrafted regions with equivalent density. PRRX1a overexpression significantly reduced hOPC proliferation compared to mCherry (7.8% ± 1.8% versus 16.3% ± 2.3%; n = 5 per group, p < 0.05, one-way ANOVA, Dunnett's post-test). In contrast, PRRX1b overexpression did not significantly impair proliferation (16.4% ± 3.1%).

Progressive Migration and Colonization of Shiverer White Matter Is Inhibited by PRRX1a

To determine whether the reduction in cell density and migration at 12 weeks was due to reduced rates of migration and colonization, we euthanized a second cohort of transplanted animals at 4 weeks. Migration and cell engraftment of mCherry hOPCs were substantially reduced compared with the rates at 12 weeks (Figures 3B and 3C). In PRRX1a-transplanted animals, the distribution of hOPCs at 4 weeks was similar to that at 12 weeks. This indicated that PRRX1a-overexpressing cells did not undergo progressive expansion and engraftment.

We hypothesized that PRRX1a-mediated arrest of *shiverer* colonization was due to induced quiescence and that active

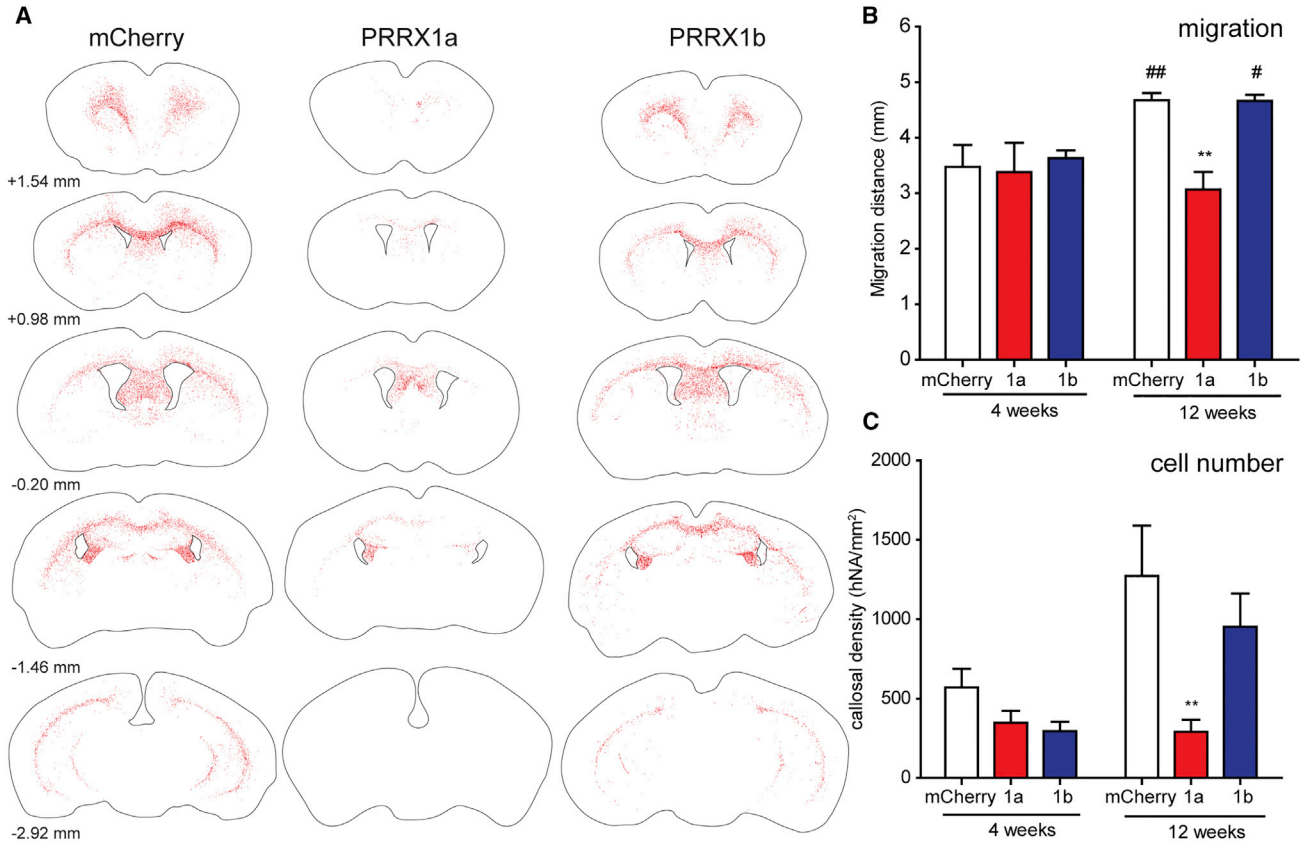

Figure 3. PRRX1 Reduces Engraftment by hOPCs *In Vivo*

hOPCs infected with PRRX1a, PRRX1b, or mCherry LV were transplanted bilaterally into the corpus callosum of postnatal day 2–3 *shiverer/rag2* mice. Mice were sacrificed 4 or 12 weeks following implantation.

(A) Total rostrocaudal dissemination of human nuclear antigen-positive cells (red dots) was assessed and plotted relative to bregma (according to Paxinos and Franklin, 2004).

(B and C) Average rostrocaudal migration distance (B, in millimeters) and hNA$^+$ cell density in the engrafted corpus callosum (C, in cells per square millimeter) of human (hNA) cells were quantified at 4 and 12 weeks after implantation.

Mean ± SEM, n = 4–9 per group; $^{**}p < 0.01$ versus mCherry, $^{\#}p < 0.05$, $^{\#\#}p < 0.01$ versus 4 weeks, two-way ANOVA, Bonferroni's post-test.

hOPCs would divide more rapidly and outcompete quiescent PRRX1a$^+$ hOPCs when transplanted into the same microenvironment. To test this hypothesis, we infected separate hOPC cultures isolated from the same donor with either mCherry or PRRX1a-FLAG LV. Cells were mixed (1:1 ratio) immediately before unilateral implantation (n = 5) (Figure S3A). At 4 weeks, we observed hNA$^+$ cells clustered at the implantation site and migrating hNA$^+$ cells across the corpus callosum (Figure S3B). At the site of injection, >99% of hNA$^+$ cells colabeled with mCherry. A few cells lacked detectable mCherry or PRRX1-FLAG-expression and likely represented uninfected hOPCs or possible silenced LV. On the contralateral side, all hNA$^+$ cells expressed mCherry and morphologically resembled migrating bipolar precursors. We did not observe FLAG immunoreactive PRRX1a$^+$ hOPCs in either site across five animals. In contrast, 11 animals were engrafted with hOPCs isolated from five human samples, with each successfully yielding PRRX1a-FLAG$^+$ cells upon sectioning at 4 and 12 weeks post-transplant. The complete absence of PRRX1a-FLAG$^+$ cells following mixed transplantation using matched donors indicates that the mCherry-infected hOPCs outcompeted PRRX1a$^+$ hOPCs *in vivo*, possibly by competition for limited trophic support.

PRRX1 Does Not Substantially Promote Myelination by hOPCs

A possible explanation for reduced migration and engraftment following PRRX1 overexpression was precocious differentiation. At 12 weeks, we found no difference in the proportion of OLIG2$^+$ cells among engrafted human cells (mCherry, 66.5% ± 4.2%; PRRX1a, 81.0% ± 4.2%; PRRX1b, 83.4% ± 7.0%) (Figures 4C and 4D). We did not observe differences in the proportion of CC1$^+$ oligodendrocytes among OLIG2$^+$hNA$^+$ cells (24.6% ± 3.0% and 25.4% ± 3.4% for PRRX1a/b, respectively, versus 19.5% ± 2.0%; n = 4–8 per group) (Figure 4F). We observed a significant decrease in the proportion of hNG2$^+$ hOPCs following PRRX1 overexpression (35.0% ± 2.6% and 30.3% ± 3.3% for PRRX1a/b, respectively, versus 46.3% ± 0.9%) (Figures 4D and 4H). There was no difference in human GFAP$^+$ astrocyte

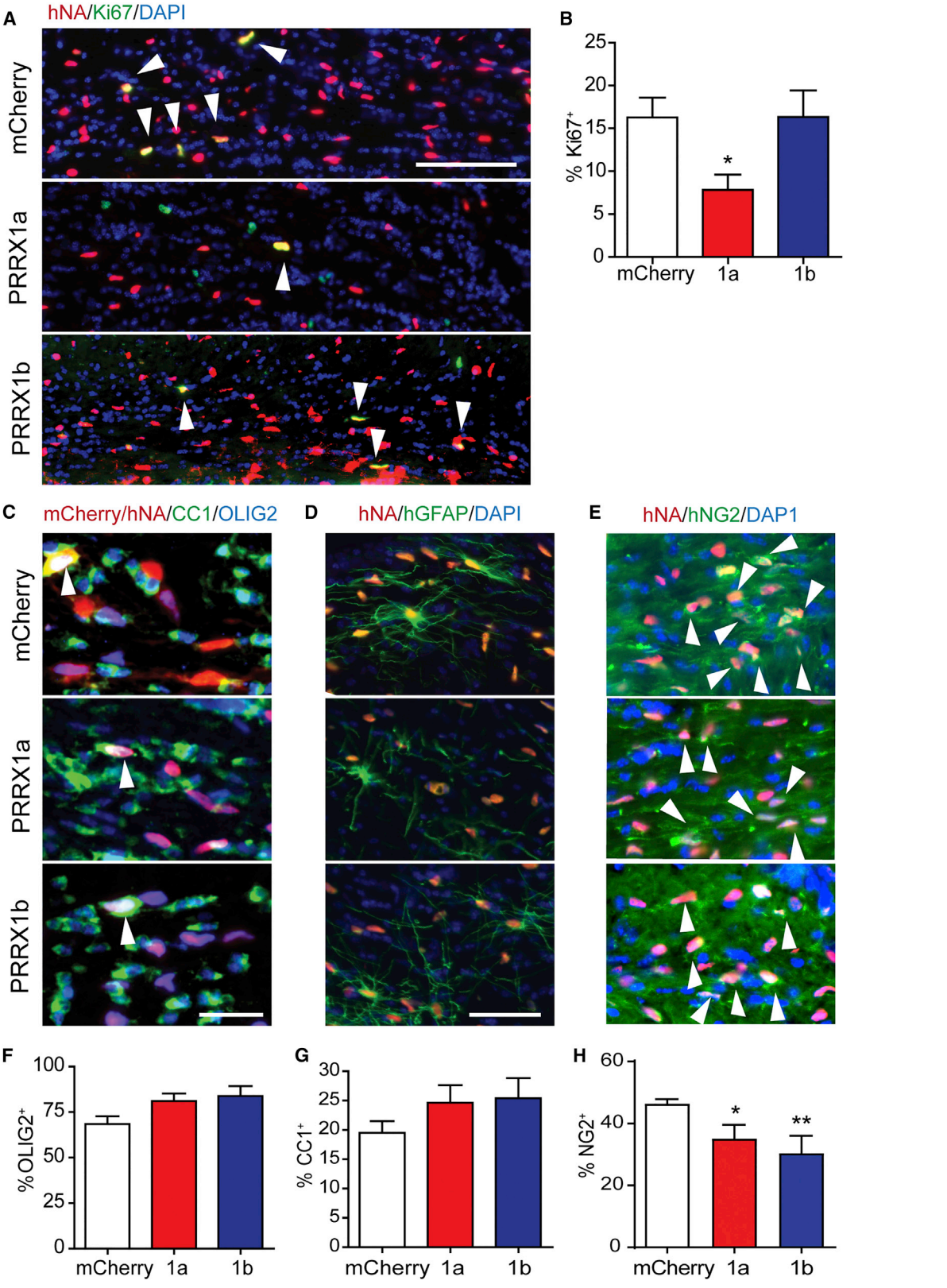

(legend on next page)

differentiation between groups (Figure 4D). In all three groups, we observed a similar distribution of human astrocytes throughout the corpus callosum, similar to previous observations (Sim et al., 2011). Altogether, these observations suggest that PRRX1 did not induce differentiation but instead acted to decrease the available pool of progenitors as a consequence of reduced cell-cycle entry and migration and thereby prevented effective engraftment.

PRRX1 Induces a Quiescent-like Gene Expression Signature

We next investigated the transcriptional mechanisms by which PRRX1 regulated hOPC proliferation and migration. We performed RNA sequencing (RNA-seq) analysis 2 days following infection with either PRRX1a/b or mCherry LV (n = 3, patient samples). Differential gene expression analysis identified more than 1,500 genes upregulated by PRRX1 compared to mCherry ($q < 0.05$) (Figure 5A). We found profound and highly significant downregulation of cell-cycle-related genes (cell-cycle term gene ontology [GO]: 0007049, $p = 5.4 \times 10^{-68}$). Almost all GO terms identified involved the regulation of cell division, proliferation, DNA replication, and cell cycle, indicating that the most profound effect of PRRX1 was to repress the cell cycle.

Most genes were similarly regulated by PRRX1a and PRRX1b overexpression (Figure 5A). To investigate splice-specific PRRX1-dependent expression, we used the PRRX1 transcript level as an additional covariate. We found that PRRX1a and PRRX1b induced the differential regulation of 177 genes (PRRX1a versus PRRX1b, $q < 0.05$). A direct comparison of the PRRX1a/b transcriptomes revealed increased expression of 24 genes associated with migration following PRRX1b overexpression (ARC, MMP9, etc.), while only 10 genes were downregulated (Figure S4A). PRRX1b upregulated a significant number of genes associated with cell migration and locomotion (GO: 004001, $p = 4.21 \times 10^{-11}$). This is consistent with PRRX1b overexpression leading to a more promigratory phenotype *in vitro* and following transplantation versus PRRX1a. Among PRRX1a-specific migration-associated transcripts, the laminin receptor integrin β4 (ITGB4) was differentially upregulated by PRRX1a relative to PRRX1b and mCherry, while seizure protein 6-like (SEZ6L) was downregulated (Figure S4C). Integrin α6β4 is not typically expressed by OPCs but can mediate stable adhesion with basement membranes, while cell surface protein SEZ6L is an OPC-expressed transcript that is downregulated during differentiation (Pol et al., 2017; Zhang et al., 2014).

Next, we performed gene set enrichment analysis (GSEA) using the MSigDB C2 database of ~5,000 gene sets (Subramanian et al., 2005). We noted that the profile of PRRX1a$^+$ cells resembled that of the response to BMP2 signaling ($q = 1.5 \times 10^{-4}$ and 1.3×10^{-5} for up- and downregulated targets, respectively) (Lee et al., 2007) (Figure 5B). Furthermore, we observed that the PRRX1 gene signature was significantly enriched for genes responsive to interferon stimulation (ZHANG_INTERFERON_RESPONSE, $q = 4.8 \times 10^{-7}$, Zhang et al., 2005; DER_IFN_GAMMA _RESPONSE_UP, $q = 4.1 \times 10^{-6}$, Der et al., 1998; and SANA_RESPONSE_TO_IFNG_UP, $q = 8.1 \times 10^{-7}$, Sana et al., 2005) (Figure 5C). As such, these data suggested that PRRX1 overexpression has a similar mode of action to BMP and interferon signaling in hOPCs.

We also found common inductive and repressive targets between PRRX1a and transcription factor FOXO3 ($q = 1.4 \times 10^{-7}$) (Delpuech et al., 2007). FOXO3 is upregulated in quiescent stem cells (Cheung and Rando, 2013) and is required for adult NPC maintenance (Paik et al., 2009; Renault et al., 2009). Among the top 20 most significantly enriched signatures was the regulation of quiescence-associated transcripts in CD34$^+$ hematopoietic stem cells in quiescent versus dividing phenotypes ($q = 7.5 \times 10^{-31}$) (Graham et al., 2007) (Figure 5D). Finally by GSEA, we identified significant enrichment of a consensus quiescent stem cell gene expression signature following PRRX1a overexpression (Figures 5E and 5F) (Cheung and Rando, 2013).

Among quiescence genes, we noted the downregulation of cell-cycle components. We confirmed the differential regulation of these by qRT-PCR (Figure 5G) (n = 3 fetal samples). Altogether, the gene expression establishes that PRRX1a overexpression induced quiescence in hOPC and suggested that PRRX1a may be regulated by BMP or interferon-gamma (IFN-γ) treatment.

Cytokine-Induced Quiescence Upregulates PRRX1 Expression in hOPC

Both IFN-γ and BMP signaling are involved in the regulation of progenitor quiescence (Tanner et al., 2011; Mira et al., 2010). As in rodent OPCs, IFN-γ treatment did not induce hOPC apoptosis at a low dose (cleaved caspase-3, up to 10 ng/mL). IFN-γ significantly reduced BrdU incorporation (20% ± 1.8% versus 35% ± 4.6%; n = 3 per group, $p < 0.05$ by paired Student's t test) (Figures 6A and 6B). Flow cytometry-based cell-cycle analysis revealed a 61% ± 2% reduction in S-phase entry following 24-hr treatment with IFN-γ (n = 2 fetal samples) (Figure S5).

Similar to rodent NPCs, we found that BMP treatment reduced the proportion of 5-Ethynyl-2'-deoxyuridine (EdU)$^+$ hOPCs

Figure 4. PRRX1 Alters Proliferation, but Not Differentiation, of hOPCs *In Vivo*

The fate and rate of hOPC differentiation was determined at 12 weeks post-implantation.

(A) Human nuclear antigen-positive (hNA$^+$) cells (red) and Ki67 (green) in corpus callosum (white arrowheads indicate double-labeled cells).

(B) Percentage of Ki67$^+$ among transplanted hNA$^+$ was determined as a measure of proliferation (n = 5–9 per group; *$p < 0.05$ versus mCherry, one-way ANOVA, Dunnett's post-test).

(C–H) Serial sections were stained for oligodendrocyte lineage-expressed OLIG2 (blue) and CC1, a marker of post-mitotic oligodendrocytes (green) (arrowheads indicate triple-labeled cells) (C). The extent of OLIG2$^+$ lineage commitment (F), and the rate of human CC1$^+$ oligodendrocyte differentiation among hNA$^+$OLIG2$^+$ cells was determined (G) (mean ± SEM, n = 4–9 per group). (D) Human astrocyte differentiation by transplanted cells was similar between groups (human-specific GFAP antibody). (E) hOPC fate was determined using human-specific NG2 antibody (hNG2) and quantified (H) (*$p < 0.05$ and **$p < 0.01$ versus mCherry, one-way ANOVA, Dunnett's post-test).

Scale: 100 μm (A), 25 μm (C), and 50 μm (D).

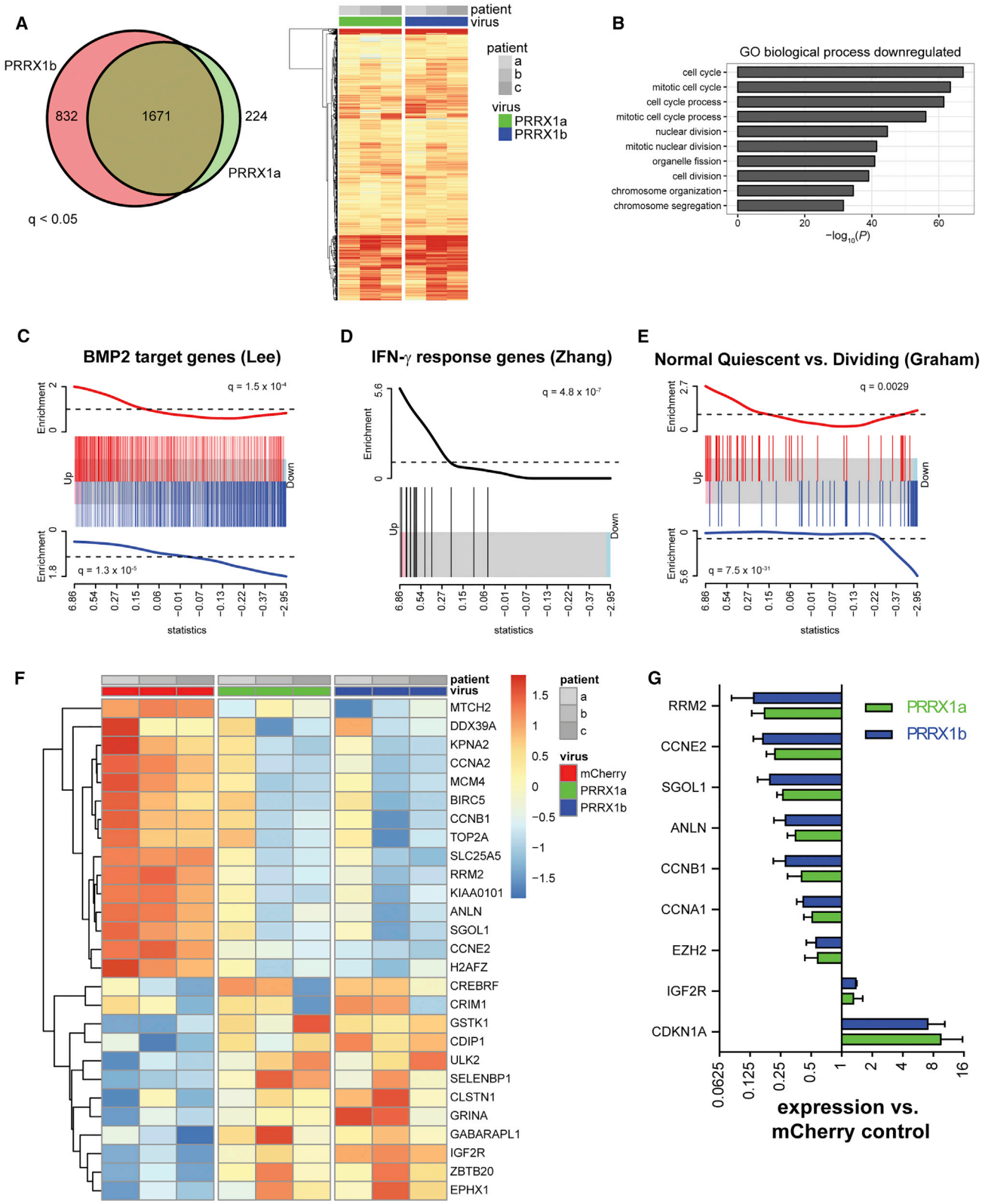

(legend on next page)

by 27% ± 4% (Figure S5). Because BMP induces astrocyte differentiation from hOPCs (Sim et al., 2011), we further investigated hOPC fate and OLIG2$^+$ hOPC proliferation (Figure S6). Although BMP treatment increased the proportion of GFAP$^+$ cells, the fraction of OLIG2$^+$ cells remained greater than 75% at 24 hr (89% ± 4.1% to 78% ± 3.3%, n = 2 fetal samples). Consistent with induced hOPC quiescence, BMP treatment significantly reduced the fraction of dividing OLIG2-expressing EdU$^+$ cells (n = 3 fetal samples) (Figure S6), thus indicating that both IFN-γ and BMP can inhibit cell-cycle entry in hOPCs.

Given the coregulation of PRRX1 and both BMP2 and IFN-γ target genes, we next asked whether PRRX1 was regulated by BMP or IFN-γ. IFN-γ increased PRRX1a and PRRX1b mRNA (1.66- ± 0.03-fold and 1.96- ± 0.15-fold, respectively, at 10 ng/mL IFN-γ relative to untreated control; n = 3 per group, $p < 0.005$, one-way ANOVA, Dunnett's post-test) (Figure 6C). Likewise, 50 ng/mL BMP2 and BMP4 upregulated both isoforms by >4-fold. Specifically, BMP2 increased PRRX1a and PRRX1b levels 4.82 ± 0.50 and 4.28 ± 0.81, respectively (n = 3 per group, $p < 0.05$, paired Student's t test). BMP4 increased PRRX1a and PRRX1b levels 4.61 ± 0.19 and 4.67 ± 0.52, respectively, compared to controls (n = 4 per group, $p < 0.001$, paired Student's t test) (Figure 6D). These data indicate that endogenous PRRX1 mRNA was upregulated by cytokines capable of inducing hOPC quiescence.

PRRX1 Is Necessary for IFN-γ-Induced Quiescence in hOPCs

To determine whether PRRX1 mRNA upregulation was necessary for cytokine-induced quiescence, we transfected hOPCs with PRRX1 or non-targeting control (NTC) small interfering RNA (siRNA). The effect of PRRX1 knockdown (KD) on IFN-γ-induced quiescence was assessed by analysis of S-phase entry (8-hr EdU pulse). PRRX1 KD in the absence of IFN-γ did not significantly influence hOPC proliferation (0.90 ± 0.08 mitotic index, defined as the percentage of EdU positive relative to NTC control, n = 3 fetal samples). As expected, IFN-γ reduced the mitotic index of hOPCs transfected with NTC siRNA by 46% (0.54 ± 0.03, n = 4 fetal samples) (Figures 6E and 6F). PRRX1 KD significantly increased the mitotic index of IFN-γ-treated cells, increasing by 21% (0.69 ± 0.02, paired t test, $p < 0.001$). The effect of PRRX1 siRNAi on IFN-γ-induced cell-cycle arrest was verified using two separate PRRX1 siRNAs, which similarly increased proliferation following cytokine treatment (0.67 ± 0.06 and 0.64 ± 0.01, respectively, n = 3).

To better understand the mechanisms by which PRRX1 regulates hOPCs, we performed RNA-seq analysis following siRNA and/or IFN-γ treatment (Figure S7). RNA-seq confirmed PRRX1 KD (77% KD, $q = 7.3 \times 10^{-9}$). 646 and 796 genes were significantly regulated by PRRX1 KD in the presence of PDGF-AA and neurotrophin-3 (NT-3) alone and following IFN-γ treatment, respectively ($q < 0.05$). In actively dividing hOPCs, PRRX1 KD resulted in upregulation of cell proliferation genes (GO: 0008283, topGO analysis; $q = 4 \times 10^{-7}$) and locomotion genes (GO: 0040011, $q = 8.0 \times 10^{-5}$), consistent with the observed repressive effects of PRRX1 (Figure S7). Basal PRRX1 expression was necessary for expression of cholesterol biosynthesis genes (HORTON_SREBF_TARGETS, q = 0.0059), and PRRX1 KD resulted in small but significant downregulation of oligodendrocyte lineage genes (SOX10 and OLIG2) and differentiation genes (MBP and PLP1) (Figure S7). Importantly, PRRX1 KD in the presence of IFN-γ resulted in downregulation of genes associated with the IFN-γ-response (SANA_RESPONSE_TO_IFNG_UP, $q = 1.9 \times 10^{-5}$) (Figure S7) and establishes a role for PRRX1 in meditating the IFN-γ-dependent responses.

PRRX1 Is Expressed by Ki67-Negative OPCs following Demyelination and Induced by IFN-γ

To further investigate PRRX1 expression *in vivo*, we performed semiquantitative fluorescence *in situ* hybridization. As expected, we observed high levels of Prrx1 mRNA in the adult mouse subventricular zone (Shimozaki et al., 2013). At postnatal day 7, we found that many cells in mouse white matter expressed low levels of Prrx1 (Figure 7A). In the corpus callosum, dividing OPCs defined as Pdgfra$^+$Ki67$^+$ cells (white arrows) were largely Prrx1 negative. In contrast, a small subpopulation of Pdgfra$^+$ OPCs expressed Prrx1, with most of these cells negative for Ki67 (Figure 7A, yellow arrows). While Prrx1 expression in non-OPCs decreased significantly with age, the pattern of Prrx1 expression in OPCs became more pronounced after the peak of oligodendrocyte generation. In postnatal day 28 corpus callosum and in aged adult spinal cord at 24 weeks, Prrx1 expression was largely restricted to Pdgfra$^+$Ki67$^-$ OPCs (Figures 7B and 7D). Dividing Ki67$^+$ OPCs were negative or Prrx1^{low} (Figure 7C). Next, we examined the expression of Prrx1 mRNA following demyelination induced by lysolecithin

Figure 5. PRRX1 Overexpression Induces a Gene Signature Associated with Quiescence

RNA-seq analysis was performed 48 hr after infection with PRRX1 or mCherry LV (n = 3 individual patient samples).

(A) Differential gene expression analysis identified >1,500 genes upregulated compared to mCherry hOPCs ($q < 0.05$). Venn diagram shows the high extent of overlap between genes upregulated between PRRX1a and PRRX1b. Likewise, the heatmap of all upregulated genes reflects strong correlation between PRRX1a and PRRX1b transcriptional responses (expression relative to matched mCherry-infected hOPCs; increasing intensity of red indicates upregulation).

(B) Gene ontology-based over-representation analysis revealed that cell-cycle-related biological process terms were significantly downregulated in response to PRRX1 overexpression.

(C–E) Gene set enrichment analysis showed coordinated regulation of transcripts associated with BMP2 (C), IFN-γ (D), and quiescence (E). Barcode plots are shown, and the x axis is the rank order of hOPC genes by the F-test statistic in response to PRRX1a expression. Red bars indicate the position of upregulated genes, and blue bars indicate the downregulated genes in each gene set. The red and blue traces above and below show relative enrichment of up- and downregulated genes, respectively (q value is shown).

(F) Heatmap of significantly regulated genes associated with the stem cell quiescence signature (Cheung and Rando, 2013). Scale indicates expression relative to median level across RNA samples.

(G) qPCR of cell-cycle genes following PRRX1 infection (mean ± SEM, n = 3).

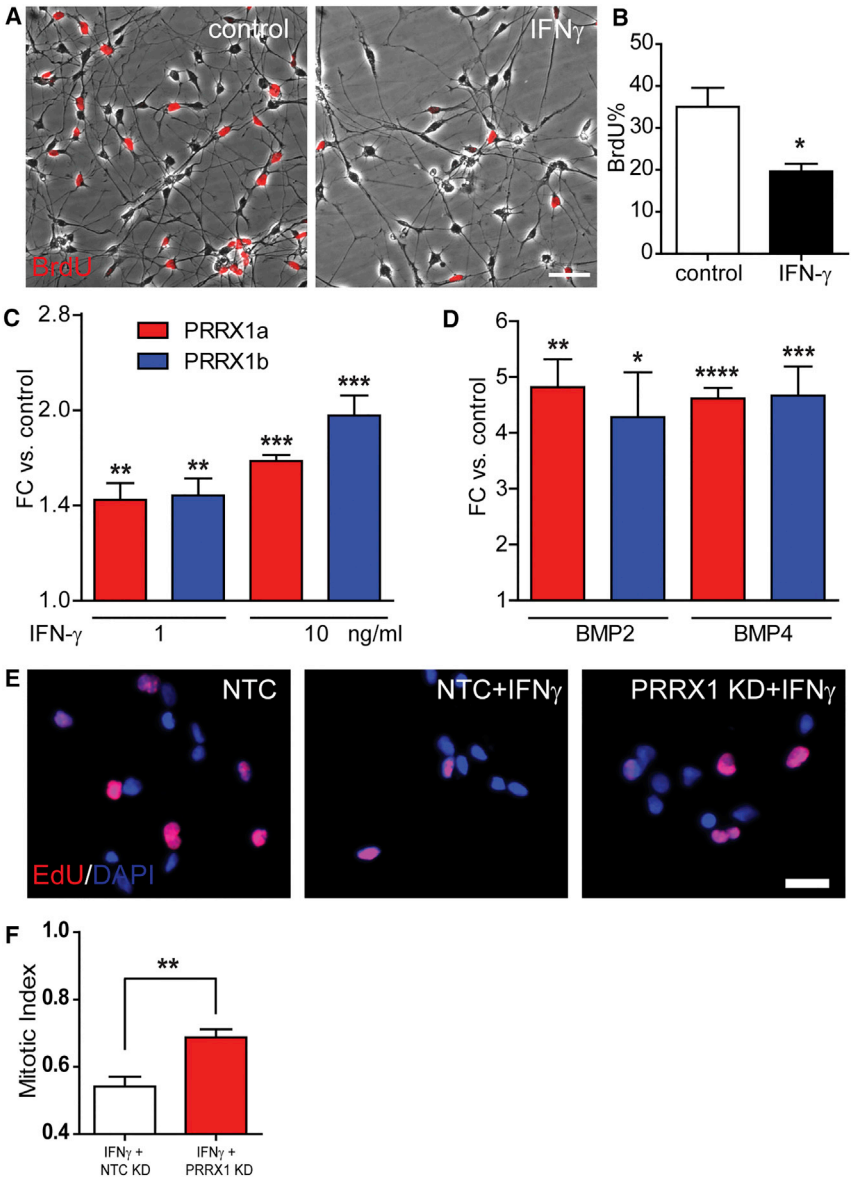

Figure 6. IFN-γ and BMP Induce Endogenous PRRX1 Expression

(A) Phase contrast images of hOPCs overlaid with BrdU immunofluorescence in control and after IFN-γ treatment for 7 days (10 ng/mL).

(B) Quantification of proliferating hOPC after IFN-γ treatment.

(C and D) Cytokine treatment significantly increased PRRX1a and PRRX1b mRNA following exposure to IFN-γ (C) or 50 ng/mL BMP (D) (n = 3–4 fetal samples each; *p < 0.05, **p < 0.01, ***p < 0.001, one-way ANOVA).

(E) To determine whether PRRX1 upregulation was necessary for IFN-γ-induced quiescence, fetal hOPCs were transfected with NTC (non-targeting control) or PRRX1 siRNA. The effect of PRRX1 knockdown on IFN-γ-induced hOPC quiescence was assessed by EdU (8-hr pulse).

(F) Mitotic index of IFN-γ-treated cells was calculated relative to the untreated matched hOPCs (mean ± SEM, n = 4 fetal samples; **p < 0.01, paired t test).

Scale: 100 μm (A) and 50 μm (E).

injection into the spinal cord of 24-week-old adult mice. We examined the expression of Prrx1 at 5 days post-lesion (dpl), because OPCs at this stage have been recruited from surrounding white matter and are actively dividing in and around the lesion (Sim et al., 2002) (data not shown). Prrx1 was substantially upregulated within the lesion and was expressed by multiple cell types, including Pdgfra^{+} OPCs (Figure 7E). Prrx1 expression was predictive of the Ki67 status of OPCs, with Prrx1^{low}Ki67^{+} dividing OPCs found predominantly at the lesion edge and Prrx1^{high}Ki67^{-} quiescent OPCs in the lesion center. Finally, to determine whether IFN-γ could upregulate Prrx1 expression *in vivo*, we coinjected IFN-γ into demyelinating lesions (300 U). At 5 dpl, Prrx1 was strongly enhanced throughout the lesion and surrounding tissue (Figure 7F). OPC division was inhibited by IFN-γ, with almost all Pdgfra^{+} cells within the lesion exhibiting a Prrx1^{high}Ki67^{-} phenotype, suggesting that IFN-γ-mediated signaling could induce Prrx1 and induce OPC quiescence.

DISCUSSION

Adult OPCs are considered quiescent due to their slow rate of proliferation (Psachoulia et al., 2009) and reduced expression of cell-cycle genes (Belachew et al., 2002; Lin et al., 2009). Here, we show that quiescence can be induced in fetal hOPCs by PRRX1 overexpression and that induction of quiescence by cytokine treatment depends on PRRX1 upregulation. Prrx1 mRNA expression in mouse was associated with non-dividing OPCs and was induced following demyelination. These data provide insight into the regulation of cell-cycle dynamics and quiescence in hOPCs that may help uncover the mechanisms important for their homeostasis and activation following injury.

The principal effect of PRRX1 on hOPCs was the induction of a reversible cell-cycle arrest. We observed a dominant effect of PRRX1a both in culture and following transplantation. The expression data demonstrate that both PRRX1 isoforms are upregulated in OPCs compared to NPCs and subsequently downregulated during oligodendrocyte differentiation. Although forced expression of PRRX1 induced cell-cycle arrest, it did not prevent the progression of cells to mature oligodendrocytes, because comparable numbers of oligodendrocytes were observed *in vitro* and *in vivo*, respectively. Previously, PRRX1 expression in human and rodent NPCs induced some features of OPC fate (Wang et al., 2014; Shimozaki et al., 2013). Similar results were reported in a study by Mira et al. (2010), in which a substantial proportion of

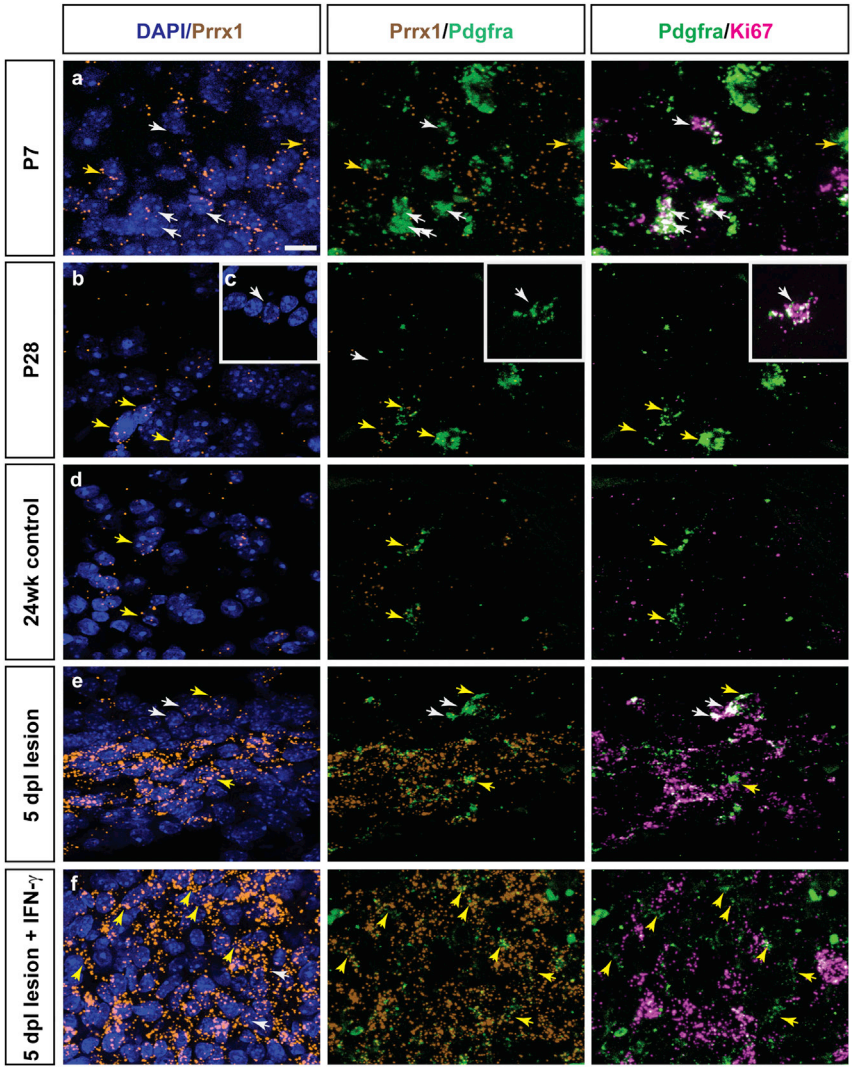

Figure 7. Prrx1 mRNA Expression in Mouse OPCs and following Demyelination

PRRX1 expression was analyzed in mouse brain and spinal cord during normal development and following demyelination.

(A–C) Triple-labeled fluorescence *in situ* hybridization (FISH) of postnatal day 7 (A) and day 28 (B and C) in mouse corpus callosum: Prrx1 mRNA (orange), Pdgfra mRNA (green), and Ki67 mRNA (pink). White arrows denote Prrx1^{low} or Prrx1-negative Pdgfra^{+} OPCs that coexpressed Ki67, a marker of proliferating cells. Yellow arrows denote Prrx1^{high} Pdgfra^{+} OPCs. These cells were typically Ki67 negative.

(D) 24-week adult mouse spinal cord ventral white matter.

(E) 24-week adult mouse spinal cords were lesioned via direct injection of lysolecithin.

(F) Coinjection of lysolecithin and IFN-γ into ventral white matter. Animals were sacrificed at 5 days post-lesion (dpl) (n = 3 per group).

Scale: 20 μm.

quiescent (Ki67^{-}) NPCs were found to express oligodendroglial and astrocytic differentiation markers. This is further evidence that quiescence in OPCs is distinct from processes regulating terminal differentiation, which is not an obligatory consequence of cell-cycle exit (Levine et al., 2001). Given that PDGFαR^{+} hOPCs represent a mixture of different developmental stages or cell-cycle status (Dietz et al., 2016), it is also possible that PRRX1 regulates quiescence in a subset of OPCs. Only a small proportion of fetal hOPCs expressed high levels of PRRX1 by single-cell RNA-seq, and only a subpopulation of OPCs express PRRX1 during mouse development, which suggests that this transcript may be differentially activated by the local environment or niche.

PRRX1 induced profound repression of cell-cycle-associated transcripts. Downregulation of CDK2/cyclin E (CCNE1) corresponds with their essential role in OPC proliferation (Belachew et al., 2002). Likewise, PRRX1 expression was associated with highly significant upregulation of cell-cycle inhibitors p21^{CIP1} (CDKN1A) and p15^{INK4B} (CDKN2B). Surprisingly, we noted significant downregulation of other inhibitors, such as p57^{KIP1} (CDKN1B) and p16^{INK4A} (CDKN2A). While p21 and p57 are often coordinately regulated *in vitro*, they are known to have distinct and non-redundant roles in OPCs (Zezula et al., 2001). The upregulation of p21 is consistent with quiescence, as observed in NPCs (Kippin et al., 2005), and downregulation of p57 may represent a resetting of the oligodendrocyte timer (Durand et al., 1998), thereby providing a stable source of progenitor cells capable of future expansion and differentiation. PRRX1 is a known inducer of epithelial-mesenchymal transition (EMT) in chick (Ocaña et al., 2012). PRRX1 does not induce expression of known mesodermal transcription factors in hOPCs. Likewise, although PRRX1 can induce SOX9 expression (Reichert et al., 2013), we did not observe any effect in hOPCs. The pattern of PRRX1 target genes appears to be tissue and cell type specific.

Our transcriptional analyses implicated PRRX1 as a target gene for both BMP- and IFN-γ-induced quiescence. While prolonged BMP treatment of rodent and hOPCs induces astrocyte differentiation (Mabie et al., 1997; Sim et al., 2006, 2011), brief BMP exposure induces a transient state before astrocytic commitment that can revert OPCs to a multipotent stem cell-like state characterized by SOX2 induction, chromatin remodeling, and increased neurogenic capacity (Kondo and Raff, 2000, 2004). Our data suggest that during the induction of this transient state, PRRX1 expression is upregulated, along with SOX2. BMP4 treatment of NPCs is known to induce reversible quiescence (Mira et al., 2010) and has been shown to upregulate PRRX1 mRNA (Martynoga et al., 2013). In that study, NFIX was identified as a key regulator of NPC quiescence. Therefore, it is intriguing that chromatin immunoprecipitation sequencing

(ChIP-seq) revealed NFIX is bound directly to the promoter of PRRX1, suggesting that PRRX1 may partly contribute to BMP-induced quiescence in NPCs. This parallels with observations in other systems in which PRRX1 expression is induced by BMP (Ocaña et al., 2012; Salazar et al., 2016).

However, IFN-γ-induced PRRX1 upregulation appears to be relatively OPC specific. PRRX1 upregulation was not observed following IFN-γ treatment in several other peripheral cell types (Johnson-Huang et al., 2012; Calderon et al., 2008; Banno et al., 2003; Tassiulas et al., 2004), including microglia (Rock et al., 2005). IFN-γ induces quiescence in rodent glia (Agresti et al., 1996; Tanner et al., 2011), and at high doses, it causes cytotoxicity (Vartanian et al., 1995; Baerwald and Popko, 1998; Horiuchi et al., 2006; Wang et al., 2010). Excessive IFN-γ levels are known to induce severe hypomyelination in CNS development (Corbin et al., 1996; LaFerla et al., 2000) and demyelination (Horwitz et al., 1997). Enforced IFN-γ expression in adult brain impaired remyelination due to either reduced OPC proliferation or differentiation (Lin et al., 2006). In MS lesions, IFN-γ mRNA is associated with perivascular inflammatory cuffs (Woodroofe and Cuzner, 1993), which is likely in apposition with migrating OPCs, which use brain microvasculature to migrate in developing brain (Tsai et al., 2016). There is a clear pathogenic role of IFN-γ in MS (Popko et al., 1997). For example, IFN-γ treatment resulted in a severe exacerbation of MS (Panitch et al., 1987). IFN-γ levels are elevated before exacerbations and remain elevated in progressive MS, suggesting a potential pathogenic role for chronic low levels of IFN-γ (Beck et al., 1988). In this study, we found that Prrx1 mRNA was upregulated in OPCs following demyelination and further induced by IFN-γ treatment. While the expression of PRRX1 has not been assessed in MS lesions, the induction of pathological quiescence by cytokine-mediated PRRX1 upregulation may prevent effective OPC recruitment in MS lesions by impairing proliferation and migration away from blood vessels.

We found that both PRRX1 variants impaired proliferation *in vitro* but that only PRRX1a was sufficient to reduce migration. PRRX1a influenced hOPC engraftment, resulting in a profound failure of cell expansion and migration *in vivo*. PRRX1a/b-specific transcripts were identified, and a significant overrepresentation of locomotion-associated genes were specifically upregulated by PRRX1b relative to PRRX1a. This is consistent with the observed negative effect of PRRX1a overexpression on migration *in vitro* and following transplantation. Furthermore, this suggests that PRRX1b may relieve the inhibitory effects of quiescence on cell motility by directly driving migration. In addition, increased expression of integrin α6β4 by PRRX1a may prevent detachment from endothelial basement membrane and thereby reduce OPC migration along microvasculature (Tsai et al., 2016). Previous studies in pancreatic cancer have indicated differential effects of PRRX1a/b, with variant-specific effects on proliferation, migration, and metastasis (Takano et al., 2016; Reichert et al., 2013). These differences were attributed to isotype-specific cofactor interactions. While identical in DNA binding homeobox domain, mouse PRRX1a (equivalent to human PRRX1b) contains an OAR domain with unknown function (Norris and Kern, 2001). PRRX1 interacts with SOX2, and its activity is greatly enhanced by SOX2 coexpression in NPCs (Shimozaki et al., 2013). The splice-specific mechanisms remain to be determined.

Following *shiverer* transplantation, hOPCs outcompete their host counterparts such that by 1 year, most OPCs were derived from donor human cells (Windrem et al., 2014). Herein, hOPC migration approximated to at least 0.2 mm/week. The 2.5- to 3-fold expansion in cell density between 8 and 12 weeks was consistent with previous studies (Sim et al., 2011; Windrem et al., 2008). In contrast, the abject failure of PRRX1a$^+$ hOPCs to engraft following mixed transplantation with mCherry$^+$ cells indicates that PRRX1 provides a strong competitive disadvantage to engrafted cells. Because PRRX1a$^+$ cells were present at 12 weeks when transplanted alone, this result suggests that PRRX1$^+$ hOPCs were either unable to compete for limiting levels of trophic factors immediately following transplantation or, after initial engraftment, that control OPCs outcompeted PRRX1$^+$ cells for trophic support and subsequently died. This is reminiscent of previous rat transplantation studies, which suggested competition between endogenous and transplanted OPCs and that a niche could only be created by depleting the host progenitor pool (Franklin et al., 1996). Among several possible trophic factors, PDGF-AA clearly regulates OPC density (Woodruff et al., 2004), and as such, PRRX1-induced changes in signaling competence might contribute to the failure of these cells to compete with control hOPCs.

Numerous studies have demonstrated that OPCs in adult human and rodent brain are relatively quiescent with a prolonged cell cycle (Belachew et al., 2002; Dawson et al., 2003; Dowling et al., 1997; Geha et al., 2010; Morris et al., 1994; Psachoulia et al., 2009; Rivers et al., 2008; Simon et al., 2011; Young et al., 2013). Cell-cycle quiescence preserves the longevity of stem cell pools to prevent excessive proliferation and exhaustion of the proliferative capacity of adult stem and progenitor cells. The linkage of progenitor exhaustion and aging has been well established in other systems (López-Otín et al., 2013). OPC exhaustion was proposed as a mechanism for failure of remyelination in a subset of chronic demyelinating MS lesions (Lucchinetti et al., 1996), and OPC recruitment is substantially delayed in aged animals following demyelination (Sim et al., 2002). Yet OPC exhaustion does not appear to be relevant in several animal modules of OPC depletion following either irradiation (Chari and Blakemore, 2002) or focal toxic injury (Penderis et al., 2003). Likewise, several studies have identified OPCs in MS lesions, albeit at densities lower than expected for successful repair (reviewed in Dietz et al., 2016). Thus, it remains unclear whether OPC exhaustion contributes to MS progression and chronic disease.

It is possible that therapies aimed at accelerating the activation of resident OPCs from a state of pathological quiescence would greatly benefit recovery in patients with MS or other demyelinated lesions. Activation of adult OPC proliferation by upregulation of the transcription factor SOX2 is required for efficient remyelination (Zhao et al., 2015). Because failure to remyelinate has been attributed to impaired activation of OPC proliferation (Wolswijk, 1998; Morris et al., 1994; Dowling et al., 1997), this

process may also occur in chronic MS lesions. However, further studies are needed to determine whether OPCs in and around chronic lesions are quiescent and whether it is the inability to overcome this pathological quiescence that impedes remyelination and repair. The results presented here suggest that PRRX1 may be an important target for such studies and those examining the regulation and maintenance of oligodendrocyte progenitors in adult brain.

STAR★METHODS

Detailed methods are provided in the online version of this paper and include the following:

- KEY RESOURCES TABLE
- CONTACT FOR REAGENT AND RESOURCE SHARING
- EXPERIMENTAL MODEL AND SUBJECT DETAILS
  - Animals and housing conditions
  - Human CD140a/PDGFαR cell culture
  - Cell Lines
- METHOD DETAILS
  - Quantitative PCR analyses
  - Lentivirus cloning and packaging
  - Lentivirus infection of hOPCs
  - Proliferation assay
  - Migration assay
  - *In vitro* differentiation
  - Transient PRRX1a expression
  - Flow cytometry cell cycle analysis
  - Transplantation into shiverer/rag2 mice
  - Immunohistochemistry
  - RNA sequencing
  - Treatment with IFN-γ and BMPs
  - siRNA-mediated PRRX1 knockdown
  - Fluorescent *in situ* hybridization (FISH)
  - Animals and spinal cord surgery
  - Statistical analysis

SUPPLEMENTAL INFORMATION

Supplemental Information includes seven figures and one table and can be found with this article online at https://doi.org/10.1016/j.celrep.2018.11.068.

ACKNOWLEDGMENTS

This work was supported by an NINDS grant (R01NS104021), NCATS (UL1TR001412), National Multiple Sclerosis Society (RG 5505-A-2 and RG 5110A1/1), the Kalec Multiple Sclerosis Foundation, the Change MS Foundation, the Skarlow Memorial Trust, and the Empire State Stem Cell Fund through a New York State Department of Health contract (C028108). J.P. received additional support from NIGMS (R25GM09545902) and NCATS (UL1TR001412-S1). The single-cell RNA-seq was carried out by Genomics Shared Resources at the Roswell Park Cancer Institute, which is supported by grants from the NIH/National Cancer Institute (P30 CA016056, RPCI Cancer Center support grant). We acknowledge the assistance of the Confocal Microscope and Flow Cytometry Facility in the School of Medicine and Biomedical Sciences, University at Buffalo. We thank Dr. Brad Poulos of the Human Fetal Tissue Repository at the Albert Einstein College of Medicine and Advanced Bioscience Resources for assistance with tissue acquisition. We thank Beverly DiCorso, Shangru Lyu, Lili Lin, Joseph E. Noble, and Nicole Wawrzyniak for technical assistance.

AUTHOR CONTRIBUTIONS

F.J.S. conceived the experiments; J.W. performed PRRX1 overexpression cell culture and *shiverer* transplantation experiments with help from M.A.O., S.U.P., K.D., J.P., and F.J.S.; D.S. performed RNAscope *in situ* hybridization experiments; A.K.S. and D.S. performed all other experiments with help from J.P., H.J.S., and M.A.O.; F.J.S. analyzed RNA-seq data; J.W., D.S., and A.K.S. analyzed all other data; and J.W. and F.J.S. wrote the manuscript. All authors read, revised, and approved the manuscript.

DECLARATION OF INTERESTS

The authors declare no competing interests.

Received: July 5, 2017
Revised: August 2, 2018
Accepted: November 16, 2018
Published: December 18, 2018

REFERENCES

Agresti, C., D'Urso, D., and Levi, G. (1996). Reversible inhibitory effects of interferon-gamma and tumour necrosis factor-alpha on oligodendroglial lineage cell proliferation and differentiation *in vitro*. Eur. J. Neurosci. *8*, 1106–1116.

Baerwald, K.D., and Popko, B. (1998). Developing and mature oligodendrocytes respond differently to the immune cytokine interferon-gamma. J. Neurosci. Res. *52*, 230–239.

Banno, T., Adachi, M., Mukkamala, L., and Blumenberg, M. (2003). Unique keratinocyte-specific effects of interferon-gamma that protect skin from viruses, identified using transcriptional profiling. Antivir. Ther. (Lond.) *8*, 541–554.

Beck, J., Rondot, P., Catinot, L., Falcoff, E., Kirchner, H., and Wietzerbin, J. (1988). Increased production of interferon gamma and tumor necrosis factor precedes clinical manifestation in multiple sclerosis: do cytokines trigger off exacerbations? Acta Neurol. Scand. *78*, 318–323.

Belachew, S., Aguirre, A.A., Wang, H., Vautier, F., Yuan, X., Anderson, S., Kirby, M., and Gallo, V. (2002). Cyclin-dependent kinase-2 controls oligodendrocyte progenitor cell cycle progression and is downregulated in adult oligodendrocyte progenitors. J. Neurosci. *22*, 8553–8562.

Birey, F., Kloc, M., Chavali, M., Hussein, I., Wilson, M., Christoffel, D.J., Chen, T., Frohman, M.A., Robinson, J.K., Russo, S.J., et al. (2015). Genetic and stress-induced loss of NG2 glia triggers emergence of depressive-like behaviors through reduced secretion of FGF2. Neuron *88*, 941–956.

Boyd, A., Zhang, H., and Williams, A. (2013). Insufficient OPC migration into demyelinated lesions is a cause of poor remyelination in MS and mouse models. Acta Neuropathol. *125*, 841–859.

Calderon, B., Suri, A., Pan, X.O., Mills, J.C., and Unanue, E.R. (2008). IFN-gamma-dependent regulatory circuits in immune inflammation highlighted in diabetes. J. Immunol. *181*, 6964–6974.

Chari, D.M., and Blakemore, W.F. (2002). Efficient recolonisation of progenitor-depleted areas of the CNS by adult oligodendrocyte progenitor cells. Glia *37*, 307–313.

Cheung, T.H., and Rando, T.A. (2013). Molecular regulation of stem cell quiescence. Nat. Rev. Mol. Cell Biol. *14*, 329–340.

Conway, G.D., O'Bara, M.A., Vedia, B.H., Pol, S.U., and Sim, F.J. (2012). Histone deacetylase activity is required for human oligodendrocyte progenitor differentiation. Glia *60*, 1944–1953.

Corbin, J.G., Kelly, D., Rath, E.M., Baerwald, K.D., Suzuki, K., and Popko, B. (1996). Targeted CNS expression of interferon-gamma in transgenic mice leads to hypomyelination, reactive gliosis, and abnormal cerebellar development. Mol. Cell. Neurosci. *7*, 354–370.

Dawson, M.R., Polito, A., Levine, J.M., and Reynolds, R. (2003). NG2-expressing glial progenitor cells: an abundant and widespread population of cycling cells in the adult rat CNS. Mol. Cell. Neurosci. *24*, 476–488.

Delpuech, O., Griffiths, B., East, P., Essafi, A., Lam, E.W., Burgering, B., Downward, J., and Schulze, A. (2007). Induction of Mxi1-SR alpha by FOXO3a contributes to repression of Myc-dependent gene expression. Mol. Cell. Biol. *27*, 4917–4930.

Der, S.D., Zhou, A., Williams, B.R., and Silverman, R.H. (1998). Identification of genes differentially regulated by interferon alpha, beta, or gamma using oligonucleotide arrays. Proc. Natl. Acad. Sci. USA *95*, 15623–15628.

Dietz, K.C., Polanco, J.J., Pol, S.U., and Sim, F.J. (2016). Targeting human oligodendrocyte progenitors for myelin repair. Exp. Neurol. *283* (*Pt B*), 489–500.

Dimou, L., Simon, C., Kirchhoff, F., Takebayashi, H., and Götz, M. (2008). Progeny of Olig2-expressing progenitors in the gray and white matter of the adult mouse cerebral cortex. J. Neurosci. *28*, 10434–10442.

Dowling, P., Husar, W., Menonna, J., Donnenfeld, H., Cook, S., and Sidhu, M. (1997). Cell death and birth in multiple sclerosis brain. J. Neurol. Sci. *149*, 1–11.

Durand, B., Fero, M.L., Roberts, J.M., and Raff, M.C. (1998). p27Kip1 alters the response of cells to mitogen and is part of a cell-intrinsic timer that arrests the cell cycle and initiates differentiation. Curr. Biol. *8*, 431–440.

Franklin, R.J.M. (2002). Why does remyelination fail in multiple sclerosis? Nat. Rev. Neurosci. *3*, 705–714.

Franklin, R.J., Bayley, S.A., and Blakemore, W.F. (1996). Transplanted CG4 cells (an oligodendrocyte progenitor cell line) survive, migrate, and contribute to repair of areas of demyelination in X-irradiated and damaged spinal cord but not in normal spinal cord. Exp. Neurol. *137*, 263–276.

Geha, S., Pallud, J., Junier, M.P., Devaux, B., Leonard, N., Chassoux, F., Chneiweiss, H., Daumas-Duport, C., and Varlet, P. (2010). NG2+/Olig2+ cells are the major cycle-related cell population of the adult human normal brain. Brain Pathol. *20*, 399–411.

Geraerts, M., Willems, S., Baekelandt, V., Debyser, Z., and Gijsbers, R. (2006). Comparison of lentiviral vector titration methods. BMC Biotechnol *6*, 34.

Graham, S.M., Vass, J.K., Holyoake, T.L., and Graham, G.J. (2007). Transcriptional analysis of quiescent and proliferating CD34+ human hemopoietic cells from normal and chronic myeloid leukemia sources. Stem Cells *25*, 3111–3120.

Horiuchi, M., Itoh, A., Pleasure, D., and Itoh, T. (2006). MEK-ERK signaling is involved in interferon-gamma-induced death of oligodendroglial progenitor cells. J. Biol. Chem. *281*, 20095–20106.

Horwitz, M.S., Evans, C.F., Mcgavern, D.B., Rodriguez, M., and Oldstone, M.B.A. (1997). Primary demyelination in transgenic mice expressing interferon-gamma. Nat. Med. *3*, 1037–1041.

Hughes, E.G., Kang, S.H., Fukaya, M., and Bergles, D.E. (2013). Oligodendrocyte progenitors balance growth with self-repulsion to achieve homeostasis in the adult brain. Nat. Neurosci. *16*, 668–676.

Johnson-Huang, L.M., Suárez-Fariñas, M., Pierson, K.C., Fuentes-Duculan, J., Cueto, I., Lentini, T., Sullivan-Whalen, M., Gilleaudeau, P., Krueger, J.G., Haider, A.S., and Lowes, M.A. (2012). A single intradermal injection of IFN-γ induces an inflammatory state in both non-lesional psoriatic and healthy skin. J. Invest. Dermatol. *132*, 1177–1187.

Kippin, T.E., Martens, D.J., and van der Kooy, D. (2005). p21 loss compromises the relative quiescence of forebrain stem cell proliferation leading to exhaustion of their proliferation capacity. Genes Dev. *19*, 756–767.

Kondo, T., and Raff, M. (2000). Oligodendrocyte precursor cells reprogrammed to become multipotential CNS stem cells. Science *289*, 1754–1757.

Kondo, T., and Raff, M. (2004). Chromatin remodeling and histone modification in the conversion of oligodendrocyte precursors to neural stem cells. Genes Dev. *18*, 2963–2972.

LaFerla, F.M., Sugarman, M.C., Lane, T.E., and Leissring, M.A. (2000). Regional hypomyelination and dysplasia in transgenic mice with astrocyte-directed expression of interferon-gamma. J. Mol. Neurosci. *15*, 45–59.

Lee, K.Y., Jeong, J.W., Wang, J., Ma, L., Martin, J.F., Tsai, S.Y., Lydon, J.P., and DeMayo, F.J. (2007). Bmp2 is critical for the murine uterine decidual response. Mol. Cell. Biol. *27*, 5468–5478.

Levine, J.M., Reynolds, R., and Fawcett, J.W. (2001). The oligodendrocyte precursor cell in health and disease. Trends Neurosci. *24*, 39–47.

Lin, W., Kemper, A., Dupree, J.L., Harding, H.P., Ron, D., and Popko, B. (2006). Interferon-gamma inhibits central nervous system remyelination through a process modulated by endoplasmic reticulum stress. Brain *129*, 1306–1318.

Lin, G., Mela, A., Guilfoyle, E.M., and Goldman, J.E. (2009). Neonatal and adult O4(+) oligodendrocyte lineage cells display different growth factor responses and different gene expression patterns. J. Neurosci. Res. *87*, 3390–3402.

López-Otín, C., Blasco, M.A., Partridge, L., Serrano, M., and Kroemer, G. (2013). The hallmarks of aging. Cell *153*, 1194–1217.

Lucchinetti, C.F., Brück, W., Rodriguez, M., and Lassmann, H. (1996). Distinct patterns of multiple sclerosis pathology indicates heterogeneity on pathogenesis. Brain Pathol. *6*, 259–274.

Mabie, P.C., Mehler, M.F., Marmur, R., Papavasiliou, A., Song, Q., and Kessler, J.A. (1997). Bone morphogenetic proteins induce astroglial differentiation of oligodendroglial-astroglial progenitor cells. J. Neurosci. *17*, 4112–4120.

Marques, S., Zeisel, A., Codeluppi, S., van Bruggen, D., Mendanha Falcão, A., Xiao, L., Li, H., Häring, M., Hochgerner, H., Romanov, R.A., et al. (2016). Oligodendrocyte heterogeneity in the mouse juvenile and adult central nervous system. Science *352*, 1326–1329.

Martynoga, B., Mateo, J.L., Zhou, B., Andersen, J., Achimastou, A., Urbán, N., van den Berg, D., Georgopoulou, D., Hadjur, S., Wittbrodt, J., et al. (2013). Epigenomic enhancer annotation reveals a key role for NFIX in neural stem cell quiescence. Genes Dev. *27*, 1769–1786.

McKenzie, I.A., Ohayon, D., Li, H., de Faria, J.P., Emery, B., Tohyama, K., and Richardson, W.D. (2014). Motor skill learning requires active central myelination. Science *346*, 318–322.

Mira, H., Andreu, Z., Suh, H., Lie, D.C., Jessberger, S., Consiglio, A., San Emeterio, J., Hortigüela, R., Marqués-Torrejón, M.A., Nakashima, K., et al. (2010). Signaling through BMPR-IA regulates quiescence and long-term activity of neural stem cells in the adult hippocampus. Cell Stem Cell *7*, 78–89.

Morris, C.S., Esiri, M.M., Sprinkle, T.J., and Gregson, N. (1994). Oligodendrocyte reactions and cell proliferation markers in human demyelinating diseases. Neuropathol. Appl. Neurobiol. *20*, 272–281.

Mourikis, P., Sambasivan, R., Castel, D., Rocheteau, P., Bizzarro, V., and Tajbakhsh, S. (2012). A critical requirement for notch signaling in maintenance of the quiescent skeletal muscle stem cell state. Stem Cells *30*, 243–252.

Norris, R.A., and Kern, M.J. (2001). The identification of Prx1 transcription regulatory domains provides a mechanism for unequal compensation by the Prx1 and Prx2 loci. J. Biol. Chem. *276*, 26829–26837.

Ocaña, O.H., Córcoles, R., Fabra, A., Moreno-Bueno, G., Acloque, H., Vega, S., Barrallo-Gimeno, A., Cano, A., and Nieto, M.A. (2012). Metastatic colonization requires the repression of the epithelial-mesenchymal transition inducer Prrx1. Cancer Cell *22*, 709–724.

Paik, J.H., Ding, Z., Narurkar, R., Ramkissoon, S., Muller, F., Kamoun, W.S., Chae, S.S., Zheng, H., Ying, H., Mahoney, J., et al. (2009). FoxOs cooperatively regulate diverse pathways governing neural stem cell homeostasis. Cell Stem Cell *5*, 540–553.

Panitch, H.S., Hirsch, R.L., Haley, A.S., and Johnson, K.P. (1987). Exacerbations of multiple sclerosis in patients treated with gamma interferon. Lancet *1*, 893–895.

Paxinos, G., and Franklin, K.B. (2004). The Mouse Brain in Stereotaxic Coordinates (Elsevier Academic Press).

Penderis, J., Shields, S.A., and Franklin, R.J. (2003). Impaired remyelination and depletion of oligodendrocyte progenitors does not occur following repeated episodes of focal demyelination in the rat central nervous system. Brain *126*, 1382–1391.

Pol, S.U., Lang, J.K., O'Bara, M.A., Cimato, T.R., McCallion, A.S., and Sim, F.J. (2013). Sox10-MCS5 enhancer dynamically tracks human oligodendrocyte progenitor fate. Exp. Neurol. *247*, 694–702.

Pol, S.U., Polanco, J.J., Seidman, R.A., O'Bara, M.A., Shayya, H.J., Dietz, K.C., and Sim, F.J. (2017). Network-based genomic analysis of human oligodendrocyte progenitor differentiation. Stem Cell Reports *9*, 710–723.

Popko, B., Corbin, J.G., Baerwald, K.D., Dupree, J., and Garcia, A.M. (1997). The effects of interferon-gamma on the central nervous system. Mol. Neurobiol. *14*, 19–35.

Psachoulia, K., Jamen, F., Young, K.M., and Richardson, W.D. (2009). Cell cycle dynamics of NG2 cells in the postnatal and ageing brain. Neuron Glia Biol. *5*, 57–67.

Reichert, M., Takano, S., von Burstin, J., Kim, S.B., Lee, J.S., Ihida-Stansbury, K., Hahn, C., Heeg, S., Schneider, G., Rhim, A.D., et al. (2013). The Prrx1 homeodomain transcription factor plays a central role in pancreatic regeneration and carcinogenesis. Genes Dev. *27*, 288–300.

Renault, V.M., Rafalski, V.A., Morgan, A.A., Salih, D.A., Brett, J.O., Webb, A.E., Villeda, S.A., Thekkat, P.U., Guillerey, C., Denko, N.C., et al. (2009). FoxO3 regulates neural stem cell homeostasis. Cell Stem Cell *5*, 527–539.

Rivers, L.E., Young, K.M., Rizzi, M., Jamen, F., Psachoulia, K., Wade, A., Kessaris, N., and Richardson, W.D. (2008). PDGFRA/NG2 glia generate myelinating oligodendrocytes and piriform projection neurons in adult mice. Nat. Neurosci. *11*, 1392–1401.

Robinson, M.D., McCarthy, D.J., and Smyth, G.K. (2010). edgeR: a Bioconductor package for differential expression analysis of digital gene expression data. Bioinformatics *26*, 139–140.

Rock, R.B., Hu, S., Deshpande, A., Munir, S., May, B.J., Baker, C.A., Peterson, P.K., and Kapur, V. (2005). Transcriptional response of human microglial cells to interferon-gamma. Genes Immun. *6*, 712–719.

Rumman, M., Dhawan, J., and Kassem, M. (2015). Concise review: quiescence in adult stem cells: biological significance and relevance to tissue regeneration. Stem Cells *33*, 2903–2912.

Salazar, V.S., Gamer, L.W., and Rosen, V. (2016). BMP signalling in skeletal development, disease and repair. Nat. Rev. Endocrinol. *12*, 203–221.

Sana, T.R., Janatpour, M.J., Sathe, M., McEvoy, L.M., and McClanahan, T.K. (2005). Microarray analysis of primary endothelial cells challenged with different inflammatory and immune cytokines. Cytokine *29*, 256–269.

Sevin, C., Benraiss, A., Van Dam, D., Bonnin, D., Nagels, G., Verot, L., Laurendeau, I., Vidaud, M., Gieselmann, V., Vanier, M., et al. (2006). Intracerebral adeno-associated virus-mediated gene transfer in rapidly progressive forms of metachromatic leukodystrophy. Hum. Mol. Genet. *15*, 53–64.

Shea, K.L., Xiang, W., LaPorta, V.S., Licht, J.D., Keller, C., Basson, M.A., and Brack, A.S. (2010). Sprouty1 regulates reversible quiescence of a self-renewing adult muscle stem cell pool during regeneration. Cell Stem Cell *6*, 117–129.

Shimozaki, K., Clemenson, G.D., Jr., and Gage, F.H. (2013). Paired related homeobox protein 1 is a regulator of stemness in adult neural stem/progenitor cells. J. Neurosci. *33*, 4066–4075.

Sim, F.J., Zhao, C., Penderis, J., and Franklin, R.J. (2002). The age-related decrease in CNS remyelination efficiency is attributable to an impairment of both oligodendrocyte progenitor recruitment and differentiation. J. Neurosci. *22*, 2451–2459.

Sim, F.J., Lang, J.K., Waldau, B., Roy, N.S., Schwartz, T.E., Pilcher, W.H., Chandross, K.J., Natesan, S., Merrill, J.E., and Goldman, S.A. (2006). Complementary patterns of gene expression by human oligodendrocyte progenitors and their environment predict determinants of progenitor maintenance and differentiation. Ann. Neurol. *59*, 763–779.

Sim, F.J., McClain, C.R., Schanz, S.J., Protack, T.L., Windrem, M.S., and Goldman, S.A. (2011). CD140a identifies a population of highly myelinogenic, migration-competent and efficiently engrafting human oligodendrocyte progenitor cells. Nat. Biotechnol. *29*, 934–941.

Simon, C., Götz, M., and Dimou, L. (2011). Progenitors in the adult cerebral cortex: cell cycle properties and regulation by physiological stimuli and injury. Glia *59*, 869–881.

Subramanian, A., Tamayo, P., Mootha, V.K., Mukherjee, S., Ebert, B.L., Gillette, M.A., Paulovich, A., Pomeroy, S.L., Golub, T.R., Lander, E.S., and Mesirov, J.P. (2005). Gene set enrichment analysis: a knowledge-based approach for interpreting genome-wide expression profiles. Proc. Natl. Acad. Sci. USA *102*, 15545–15550.

Takano, S., Reichert, M., Bakir, B., Das, K.K., Nishida, T., Miyazaki, M., Heeg, S., Collins, M.A., Marchand, B., Hicks, P.D., et al. (2016). Prrx1 isoform switching regulates pancreatic cancer invasion and metastatic colonization. Genes Dev. *30*, 233–247.

Tanner, D.C., Cherry, J.D., and Mayer-Pröschel, M. (2011). Oligodendrocyte progenitors reversibly exit the cell cycle and give rise to astrocytes in response to interferon-γ. J. Neurosci. *31*, 6235–6246.

Tassiulas, I., Hu, X., Ho, H., Kashyap, Y., Paik, P., Hu, Y., Lowell, C.A., and Ivashkiv, L.B. (2004). Amplification of IFN-alpha-induced STAT1 activation and inflammatory function by Syk and ITAM-containing adaptors. Nat. Immunol. *5*, 1181–1189.

Tsai, H.H., Niu, J., Munji, R., Davalos, D., Chang, J., Zhang, H., Tien, A.C., Kuo, C.J., Chan, J.R., Daneman, R., and Fancy, S.P. (2016). Oligodendrocyte precursors migrate along vasculature in the developing nervous system. Science *351*, 379–384.

Vartanian, T., Li, Y., Zhao, M., and Stefansson, K. (1995). Interferon-gamma-induced oligodendrocyte cell death: implications for the pathogenesis of multiple sclerosis. Mol. Med. *1*, 732–743.

Wang, Y., Ren, Z., Tao, D., Tilwalli, S., Goswami, R., and Balabanov, R. (2010). STAT1/IRF-1 signaling pathway mediates the injurious effect of interferon-gamma on oligodendrocyte progenitor cells. Glia *58*, 195–208.

Wang, J., O'Bara, M.A., Pol, S.U., and Sim, F.J. (2013). CD133/CD140a-based isolation of distinct human multipotent neural progenitor cells and oligodendrocyte progenitor cells. Stem Cells Dev. *22*, 2121–2131.

Wang, J., Pol, S.U., Haberman, A.K., Wang, C., O'Bara, M.A., and Sim, F.J. (2014). Transcription factor induction of human oligodendrocyte progenitor fate and differentiation. Proc. Natl. Acad. Sci. USA *111*, E2885–E2894.

Welliver, R.R., Polanco, J.J., Seidman, R.A., Sinha, A.K., O'Bara, M.A., Khaku, Z.M., Santiago González, D.A., Nishiyama, A., Wess, J., Feltri, M.L., et al. (2018). Muscarinic receptor M_3R signaling prevents efficient remyelination by human and mouse oligodendrocyte progenitor cells. J. Neurosci. *38*, 6921–6932.

Windrem, M.S., Schanz, S.J., Guo, M., Tian, G.F., Washco, V., Stanwood, N., Rasband, M., Roy, N.S., Nedergaard, M., Havton, L.A., et al. (2008). Neonatal chimerization with human glial progenitor cells can both remyelinate and rescue the otherwise lethally hypomyelinated shiverer mouse. Cell Stem Cell *2*, 553–565.

Windrem, M.S., Schanz, S.J., Morrow, C., Munir, J., Chandler-Militello, D., Wang, S., and Goldman, S.A. (2014). A competitive advantage by neonatally engrafted human glial progenitors yields mice whose brains are chimeric for human glia. J. Neurosci. *34*, 16153–16161.

Wolswijk, G. (1998). Chronic stage multiple sclerosis lesions contain a relatively quiescent population of oligodendrocyte precursor cells. J. Neurosci. *18*, 601–609.

Woodroofe, M.N., and Cuzner, M.L. (1993). Cytokine mRNA expression in inflammatory multiple sclerosis lesions: detection by non-radioactive in situ hybridization. Cytokine *5*, 583–588.

Woodruff, R.H., Fruttiger, M., Richardson, W.D., and Franklin, R.J. (2004). Platelet-derived growth factor regulates oligodendrocyte progenitor numbers in adult CNS and their response following CNS demyelination. Mol. Cell. Neurosci. *25*, 252–262.

Young, K.M., Psachoulia, K., Tripathi, R.B., Dunn, S.J., Cossell, L., Attwell, D., Tohyama, K., and Richardson, W.D. (2013). Oligodendrocyte dynamics in the healthy adult CNS: evidence for myelin remodeling. Neuron *77*, 873–885.

Zezula, J., Casaccia-Bonnefil, P., Ezhevsky, S.A., Osterhout, D.J., Levine, J.M., Dowdy, S.F., Chao, M.V., and Koff, A. (2001). p21cip1 is required for the differentiation of oligodendrocytes independently of cell cycle withdrawal. EMBO Rep. *2*, 27–34.

Zhang, W., Yang, H., Kong, X., Mohapatra, S., San Juan-Vergara, H., Hellermann, G., Behera, S., Singam, R., Lockey, R.F., and Mohapatra, S.S. (2005). Inhibition of respiratory syncytial virus infection with intranasal siRNA nanoparticles targeting the viral NS1 gene. Nat. Med. *11*, 56–62.

Zhang, Y., Chen, K., Sloan, S.A., Bennett, M.L., Scholze, A.R., O'Keeffe, S., Phatnani, H.P., Guarnieri, P., Caneda, C., Ruderisch, N., et al. (2014). An RNA-sequencing transcriptome and splicing database of glia, neurons, and vascular cells of the cerebral cortex. J. Neurosci. *34*, 11929–11947.

Zhao, C., Li, W.W., and Franklin, R.J. (2006). Differences in the early inflammatory responses to toxin-induced demyelination are associated with the age-related decline in CNS remyelination. Neurobiol. Aging *27*, 1298–1307.

Zhao, C., Ma, D., Zawadzka, M., Fancy, S.P.J., Elis-Williams, L., Bouvier, G., Stockley, J.H., de Castro, G.M., Wang, B., Jacobs, S., et al. (2015). Sox2 sustains recruitment of oligodendrocyte progenitor cells following CNS demyelination and primes them for differentiation during remyelination. J. Neurosci. *35*, 11482–11499.

STAR★METHODS

KEY RESOURCES TABLE

REAGENT or RESOURCE	SOURCE	IDENTIFIER
Antibodies		
Rat anti-BrdU antibody (1:2000)	Bio-Rad / AbD Serotec	Cat# MCA2060; RRID:AB_323427
O4 primary antibody (1:25)	Dr. James Goldman (Columbia University)	N/A
Monoclonal Anti-Glial Fibrillary Acidic Protein (GFAP) antibody (G-A-5; 1:800)	Sigma-Aldrich	Cat# G3893; RRID:AB_477010
Cleaved Caspase-3 (Asp175) Antibody (1:400)	Cell Signaling Technology	Cat# 9661; RRID:AB_2341188
Human Nuclei (hNA) antibody (1:100)	Millipore Sigma	Millipore Cat# MAB1281; RRID:AB_94090
Anti-APC (Ab-7) Mouse mAb (CC-1) antibody (1:50)	Millipore Sigma	Cat# OP80; RRID:AB_2057371
Anti-Olig-2 Antibody (1:750)	Millipore Sigma	Millipore Cat# AB9610; RRID:AB_570666
Mouse Anti-GFAP Monoclonal Antibody (SMI21; 1:1000)	BioLegend (Covance)	Cat# SMI-21R-100; RRID:AB_509978
Anti-Chondroitin Sulfate Proteoglycan Antibody (9.2.27; 1:200)	Millipore	Cat# MAB2029; RRID:AB_94509
PRRX1 mouse monoclonal antibody;clone 1C2 (1:300)	OriGene	Cat# TA803112; RRID:AB_2626674
Rabbit Anti-FLAG antibody (1:200)	Sigma-Aldrich	Cat# F7425; RRID:AB_439687
Mouse Ki-67 antibody (1:25)	BD Biosciences	Cat# 550609; RRID:AB_393778
Bacterial and Virus Strains		
FUW-PRRX1a LV	This Paper	N/A
pTRIP-EF1a LV	Sevin et al., 2006	N/A
PRRX1a overexpression LV	This Paper	N/A
PRRX1b overexpression LV	Wang et al., 2014	N/A
FUW-PRRX1a LV	This Paper	N/A
Biological Samples		
Fetal brain tissue samples (17-22 week gestational age)	N/A	N/A
Chemicals, Peptides, and Recombinant Proteins		
Papain	Worthington Biochemical	Cat# LS003126
DNase	Sigma-Aldrich	Cat# D4263-5VL
poly-L-ornithine	Sigma-Aldrich	Cat# P3655-100MG
Laminin, Mouse	ThermoFisher Scientific	Cat# 23017-015
Recombinant Human PDGF-AA,	PeproTech	Cat#100-13A
Recombinant Human NT-3,	PeproTech	Cat#450-03
3,3′,5-Triiodo-L-thyronine sodium salt	Sigma-Aldrich	Cat# T5516-1MG
BrdU	Sigma-Aldrich	Cat# B5002-1G
EdU	VWR	Cat# TCE1057-50MG
DAPI	Sigma-Aldrich	Cat# D8417-5MG
Paraformaldehyde	VWR International	Cat# JTS898-7
Calcein	VWR International	Cat# 80050-600
Doxycycline hyclate	VWR International	Cat# AAJ60579-14
Recombinant Human FGF-basic	Peprotech	Cat# 100-18
ProFreeze	VWR International	Cat# 12002-076
HBSS	VWR International	Cat# 45000-458
Recombinant Human IFN-gamma	Peprotech	Cat# 300-02
Recombinant Murine IFN-γ	Peprotech	Cat# 315-05
Recombinant Human BMP-2 (CHO cell derived)	Peprotech	Cat# 120-02C
Recombinant Human BMP-4 (HeLa cell derived)	Peprotech	Cat# 120-05

(*Continued on next page*)

Continued

REAGENT or RESOURCE	SOURCE	IDENTIFIER
OCT	VWR International	Cat# 25608-930
Lipofectamine RNAiMAX transfection reagent	ThermoFisher Scientific	Cat# 13778030
Lysolecithin, L-a-Lysophosphatidylcholine from egg yolk	Sigma-Aldrich	Cat# L4129-100MG
Critical Commercial Assays		
Total RNA isolation kit	Omega Bio-Tek	Cat# 101319-242
SuperScript III Reverse transcriptase	ThermoFisher Scientific	Cat# 18080-051
Click-iT® EdU Alexa Fluor® 647 Flow Cytometry Assay Kit	ThermoFisher Scientific	Cat# C-10424
RNAscope Multiplex Fluorscent Reagent Kit V2	Advanced Cell Diagnostics	Cat# 323100
TSA® Plus Cyanine 3 kit	Perkin Elmer	Cat# NEL744E001KT
TSA® Plus Cyanine 5 kit	Perkin Elmer	Cat# NEL745E001KT
TSA Plus Fluorescein kit	Perkin Elmer	Cat# NEL741E001KT
Deposited Data		
RNA-seq	NCBI GEO	GSE122563
Experimental Models: Cell Lines		
HEK293T	ATCC	Cat# CRL-3216, RRID:CVCL_0063
Experimental Models: Organisms/Strains		
Mouse:*shiverer/rag2* mice	Windrem et al., 2008	N/A
BALB/c inbred mice	Envigo	Cat# 047
Oligonucleotides		
FITC BLOCK-iT, Fluorescent oligo	ThermoFisher Scientific	Cat# 2013
Stealth RNAi PRRX1 Human 1 (HSS143371, HSS143372, HSS143373)	ThermoFisher Scientific	Cat# 1299003
Stealth RNAi siRNA Negative Control Med GC Duplex	ThermoFisher Scientific	Cat# 12935112
RNAscope® Probe- Mm-Pdgfra-C2	Advanced Cell Diagnostics	Cat# 480661-C2
RNAscope Probe - Mm-Prrx1	Advanced Cell Diagnostics	Cat# 485231
RNAscope Probe - Mm-Mki67-C3	Advanced Cell Diagnostics	Cat# 416771-C3
Recombinant DNA		
Plasmid: FUW-M2rtTA	Addgene	Cat# 20342
ViraPower Lentiviral Packaging Mix	ThermoFisher Scientific	Cat# K497500
Plasmid: FUW-tetO-lox-NKX2.2	Wang et al., 2014	N/A
Plasmid: psPAX2	Addgene	Cat# 12260
Software and Algorithms		
Fiji/ImageJ	National Institutes of Health (NIH)	SCR_003070
Prism software	GraphPad Software	SCR_002798
AutoQuant	Media cybernetics	http://www.mediacy.com/autoquantx3
tophat (v2.1.1)	Johns Hopkins CCB	https://ccb.jhu.edu/software/tophat/index.shtml
htseq (v0.6.1)	https://doi.org/10.1093/bioinformatics/btu638	https://htseq.readthedocs.io/en/release_0.10.0/
R/Bioconductor		http://www.bioconductor.org/
DESeq2	Bioconductor	https://bioconductor.org/packages/release/bioc/html/DESeq2.html
edgeR	Bioconductor	https://bioconductor.org/packages/release/bioc/html/edgeR.html
FCS Express software (version 4)	De Novo Software	N/A
Other		
24-well transwell inserts, 6.5mm, 0.8μm	Laboratory Product Sales (LPS), Inc	Cat# 3464

CONTACT FOR REAGENT AND RESOURCE SHARING

Further information and request for resources and reagents should be directed to and will be fulfilled by the Lead Contact, Fraser Sim (fjsim@buffalo.edu).

EXPERIMENTAL MODEL AND SUBJECT DETAILS

Animals and housing conditions

All experiments were performed according to protocols approved by the University at Buffalo's Institutional Animal Care and Use Committee. Animals were maintained in specific pathogen free facility with continuous access to food and water. Health of mice were monitored regularly by veterinarian. Mice used in this study were 1-24 weeks old for development and demyelination experiments while for transplantation mice were less than 1 week. For all experimental groups involving cell transplantation, animals could not be sexed at postnatal day 1-3 and were assigned randomly to groups receiving LV-infected hOPCs. After weaning recipient mice were sexed and found to be in a ratio of 1:1.3 male:female. For other experiments examining expression of Prrx1 mRNA, both males and females were used (5:7 male:female). Mice were maintained on diurnal 12 hr light/dark cycle.

Human CD140a/PDGFαR cell culture

Fetal brain tissue samples (17-22 weeks gestational age) were obtained from patients who consented to tissue use under protocols approved by the University at Buffalo Research Subjects Institutional Review Board. Forebrain tissue was minced and dissociated using papain and DNase as previously described (Conway et al., 2012). Magnetic sorting of CD140a positive cells was performed as described (Pol et al., 2013).

Cell Lines

HEK293T cells were obtained from American Type Culture Collection (ATCC; CRL-11268). HEK293T-17 cells were grown in DMEM (Invitrogen) supplemented with 10% FBS (Invitrogen) and penicillin/streptomycin (Invitrogen) under optimum growth conditions (37°C, 5% CO_2).

METHOD DETAILS

Quantitative PCR analyses

RNA was extracted from freshly sorted human cells and after 1-4 d or indicated treatment length in culture using a total RNA isolation kit (Omega Bio-Tek). cDNA was synthesized using SuperScript III reverse transcriptase (ThermoFisher Scientific). Human-specific primers designed using NCBI Primer-BLAST or Primer Express (v1; Applied Biosystems) (Table S1)(Wang et al., 2014). GAPDH was used as a control gene. Samples were run in duplicate and gene expression was calculated by $\Delta\Delta C_t$ analysis.

Lentivirus cloning and packaging

Complete coding sequences for a flag-tagged PRRX1a and PRRX1b with additional restriction enzyme sites (*Spe*I and *Xho*I) were obtained by PCR using the following primer sequences: PRRX1b, 5′-AAATCTAGACCCATGACCTCCAGCTACGGGCACG-3′ (forward), 5′-AAACTCGAGCCTCAGTTGACTGTTGGCACCTGG-3′ (reverse); PRRX1a-flag, 5′-TTTACTAGTGACCATGACCTCCA GCTA-3′ (forward), 5′-AAACTCGAGTTACTTGTCGTCATCGTCTTTGTAGTCGAATCCGTTATGAAGCCC-3′ (reverse). PCR products were then cloned into a lentiviral backbone in place of the mCherry sequence (excised with *Spe*I and *Xho*I) (derived from pTRIP-EF1a, in Sevin et al., 2006) (gift of Abdel Benraiss, University of Rochester).

Lentiviruses were prepared as described previously (Sim et al., 2006). Briefly, following triple transfection of HEK293T cells with pTRIP and packaging plasmids pLP/VSVG (ThermoFisher Scientific) and psPAX2 (AddGene), viral supernatant was collected at 48 and 72 h. Titration of virus was performed by flow cytometry for mCherry-expressing virus and using real-time quantitative PCR for the WPRE sequence (Geraerts et al., 2006). Human primary cells were infected at 1 MOI for 24 h followed by complete media replacement unless stated otherwise.

Lentivirus infection of hOPCs

Human $CD140a^+$ OPCs were plated at 5×10^4/ml on poly-L-ornithine- and laminin-coated tissue-culture plates and cultured for 48 h in serum-free medium (SFM) supplemented with 20 ng/ml PDGF-AA and 5 ng/ml NT-3 (PeproTech). Cells were then infected with the above-described lentiviruses at 1 MOI and maintained for at least 24 h prior to subsequent experiments.

Proliferation assay

Human $CD140a^+$ OPCs were infected with lentivirus as described above and cultured for 48 h in SFM supplemented with 20 ng/ml PDGF-AA and 5 ng/ml NT-3. BrdU (30 μM, Sigma) was then added, and cells were fixed 24 h later. Cells were immunostained for BrdU (1:1000; AbD Serotec) and the percentage of $BrdU^+$ DAPI-stained nuclei was obtained from 5–6 fields for each fetal sample.

Migration assay

Human CD140a$^+$ OPCs (5 × 10^4/ml) were cultured on laminin-coated membrane inserts with 8-μm diameter pores (Corning) and infected for 24 h with lentiviruses. Cells were maintained in medium containing 20 ng/ml PDGF-AA and 5 ng/ml NT-3 for 2 d. PDGF was then removed for 24 h, and subsequently reintroduced to the bottom chamber only at 100 ng/ml. After 16 h, cells were fixed with a 4% paraformaldehyde solution and DAPI-stained nuclei were imaged (five fields per membrane) before and after cells were scraped from the top surface of the insert membrane. Migration was calculated as the number of remaining (migrated) nuclei divided by the total number of nuclei.

In vitro differentiation

Human CD140a$^+$ OPCs were maintained in culture medium containing 20 ng/ml PDGF-AA and 5 ng/ml NT-3 for 2 d after lentivirus infection. Then, PDGF-AA was removed and 40 ng/ml T3 (Sigma) was added to promote OPC differentiation for 2 d. Cells were live-stained with O4 primary antibody (1:25; ATCC), then fixed for subsequent secondary and anti-GFAP (1:500; Sigma) immunocytochemistry. Six random fields were imaged with a 20 × objective for each condition, and at least 200 total cells were counted. The density of O4$^+$ and GFAP$^+$ cells are expressed as number of cells per field. Apoptosis post-infection was assessed by staining parallel cultures with anti-cleaved caspase-3 (1:400; Cell Signaling Technology). In addition, overall viability was measured in matched cultures of hOPCs 48 hr post-infection, by live staining with calcein (3μg/mL; Millipore) and DAPI (1μg/mL; Sigma) for 30 min at 37°C. Cultures were then imaged for calcein and DAPI fluorescence with a 10x objective with >20 fields analyzed per condition (n = 3 fetal human samples).

Transient PRRX1a expression

The PRRX1 coding sequence (CDS) was cloned into FUW-tetO-lox-NKX2.2 plasmid, as described previously (Wang et al., 2014). Human CD140a$^+$ OPCs were coinfected with FUW-M2rtTA (Addgene; 20342) and FUW-PRRX1a LV, at 0.5 and 0.15 multiplicity of infection, respectively. Cells were maintained in SFM as described above and treated with doxycycline 48 hr post-infection (0.19 μM, VWR International). Media and doxycycline were replaced every other day. 0.19 μM doxycycline treatment had no effect on hOPC growth. Cultures were given a 24-hr terminal pulse of 5-bromo-2′-deoxyuridine (BrdU, 10 μM) prior to fixation for assessment of cell proliferation.

Flow cytometry cell cycle analysis

Human CD140a$^+$ OPCs were infected with lentivirus as described above and cultured for 48 h in SFM supplemented with 20 ng/ml PDGF-AA and 5 ng/ml NT-3. EdU (50 μM) was then added, and cells were collected 24 h later and processed using the Click-iT EdU Flow Cytometry Assay Kit (ThermoFisher Scientific) according to the manufacturer's protocol. DNA was stained with 1 μg/ml DAPI and cells were analyzed on a Fortessa SORP flow cytometer (BD Biosciences) and using FCS Express software (version 4; *De Novo* Software).

Transplantation into shiverer/rag2 mice

All transplantation experiments were performed using *shiverer/rag2* mice (a gift of Dr. Steven A. Goldman, University of Rochester)(Windrem et al., 2008) according to protocols approved by the University at Buffalo Institutional Animal Care and Use Committee. A total of nine fetal brain samples at 17–20 weeks gestational age were used for transplantation experiments. CD140a$^+$ hOPCs were cultured for up to 1 week in SFM containing PDGF-AA (20 ng/ml) and NT-3 (5 ng/ml) and frozen using ProFreeze (Lonza) prior to surgery. Prior to injection, cells were thawed, infected with lentiviruses, and cultured for 24-48 h before resuspending in HBSS (Corning) at 1 × 10^5/μl. To better account for human sample differences, cells from human tissue donors were often combined prior to infection and subsequent transplantation. Injections were performed as previously described (Sim et al., 2011). Briefly, postnatal day 2–3 pups were anesthetized by hypothermia and bilateral injections of 5 × 10^4 cells were made with pulled glass pipettes inserted directly through the skull into the corpus callosum (~2.5 mm posterior to bregma) to a depth of 1.1 mm. Animals were sacrificed after 4 or 12 weeks by transcardial perfusion with HBSS followed by a 4% formaldehyde solution.

Immunohistochemistry

Immunohistochemistry was performed on coronal sections (16 μm) of mouse forebrain, as previously described (Sim et al., 2011). Human cells were identified with mouse anti-human nuclei antibodies (hNA; 1:400; Millipore), and co-labeled with markers for oligodendrocytes (CC1, 1:50; OLIG2, 1:750; Millipore), astrocytes (GFAP, SMI21; 1:1000; Covance) and OPCs (hNG2, 9.2.27; 1:200; Millipore). Overexpression was detected using anti-PRRX1 (1:300; OriGene) and anti-FLAG (1:200; Sigma) antibodies. Proliferating cells were detected using antibodies against Ki67 (1:25; BD Biosciences) or BrdU (1:2000; AbD Serotec). Alexa Fluor (488, 594, and 647) secondary antibodies (ThermoFisher Scientific) were used at 1:500 dilution. Sections were imaged with a 20 × objective using an inverted fluorescence microscope (Olympus IX51). The quantification of hNA$^+$ and double-positive cells was performed by counting cells in midline and lateral regions of the corpus callosum; images from at least 9 fields containing >200 cells were collected per animal. To assess the migration of implanted cells, sections spanning from bregma +3.9 to −3.4 mm (Paxinos and Franklin, 2004) were sampled every 160 μm and immunostained for hNA. The rostrocaudal migration distance was calculated as the distance between the first and last sections containing hNA$^+$ cells.

RNA sequencing

Human fetal CD140a$^+$ OPCs were maintained in proliferative conditions with SFM supplemented with 20 ng/ml PDGF-AA and 5 ng/ml NT-3 after lentivirus infection with mCherry (control) or PRRX1a overexpression or PRRX1b overexpression, for 2 days before mRNA extraction. RNA extraction and first stand synthesis was performed as described previously (Conway et al., 2012). RNA sequencing was performed at the UB sequencing core on an Illumina HiSeq2500 using 100 cycle paired-end sequencing. Sequences were aligned to the UCSC Hg19 mouse genome using tophat (v2.1.1) and counts per gene determined using htseq (v0.6.1). R/Bioconductor was used for subsequent analysis. Following loading of read counts using *DESeq2*, fragments per kilobase per million mapped fragments (FPKM) were calculated. hOPCs isolated from three separate fetal samples between 20- and 21-week gestation age were used. *edgeR* was used for differential expression analysis of read counts (Robinson et al., 2010). Genes with low counts (less than one count-per-million) in at least three libraries were removed from the analysis, and TMM normalized to account for differences between libraries (Robinson et al., 2010). A quasi-likelihood negative bionomial generalized log-linear model was fitted and empirical Bayes F-test performed to identify differentially expressed transcripts in PRRX1-expressing hOPCs. This was preferred as it provides a robust method given the small number of biological replicates (n = 3, fetal samples). p values were controlled for multiple testing by determining the false discovery rate (FDR). Pathway analysis was performed in edgeR using gene ontology (GO) enrichment analysis, KEGG pathway enrichment analysis, and gene set enrichment analysis of Broad C2 gene sets (v5) using *camera*. Heatmaps were plotted using on expression values following variance stabilizing transformation of normalized count data (*DESeq2*).

Treatment with IFN-γ and BMPs

hOPCs were then grown in SFM supplemented with 20ng/ml PDGF-AA and 5ng/ml of NT-3 prior to and during the treatment with IFN-γ or BMP (Peprotech). For mRNA-extraction, hOPCs were treated with IFN-γ for 18 hr. For BMP2/BMP4, hOPCs were treated for 40 hr before mRNA extraction. For assessment of proliferation following cytokine treatment, hOPCs were treated with IFN-γ (0-100 ng/ml) and added at each media change. The culture was given an 18-hr terminal BrdU pulse prior to fixation and assessment of mitotic index. For assessment of cell fate, cultures were treated with cytokines for 24 hr prior to fixation. OLIG2 (Millipore) and GFAP (Covance) were stained as described above.10 random fields were imaged at 20X, and at least 500 cells were counted in each condition.

siRNA-mediated PRRX1 knockdown

Stealth RNAi molecules were obtained from ThermoFisher Scientific, three targeting human PRRX1 (HSS143371, HSS143372, HSS143373), and a non-targeting control RNAi (NTC #12935112). hOPCs were seeded at 80% confluence onto 48-well plates. 24 hr later, combined or individual siRNAs (total concentration 100 nM) were transfected using Lipofectamine RNAiMAX transfection reagent (ThermoFisher Scientific). The three individual PRRX1 siRNA reduced mRNA expression by 65 ± 3, 45 ± 5 and 76 ± 3% respectively, while the pooled siRNA reduced expressed 73 ± 7% (n = 2, human samples). hOPCs were treated with IFN-γ 10 ng/ml at 8 hr post transfection and cells fixed 24hrs later. Proliferation was assessed by measurement of EdU incorporation (8-hour terminal pulse, 10 μM EdU) using the Click-iT Plus Edu Alexa imaging kit (ThermoFisher Scientific). Experiments were performed on hOPCs from individual human fetal samples, and the mitotic index was calculated relative to cells transfected with NTC in the absence of IFN-γ. Identical experiments performed in 6-well plates were performed with subsequent RNA extraction and RNA-seq as described above (n = 2, human samples).

Fluorescent *in situ* hybridization (FISH)

Triple label FISH was performed with probes targeting *Prrx1* (GenBank: NM_011127.2), *Pdgfra* (GenBank: NM_011058.2), *Ki67* (GenBank: NM_001081117.2) mRNA using RNAscope Fluorescence V2 assay (Advanced Cell Diagnostics) according to the manufacturer's instructions. Postnatal day 7 (p7), day 28, and 24-week-old mice were euthanized and perfused with 0.9% saline followed by 4% paraformaldehyde. Dissected mice brains and spinal cords were cryopreserved in sucrose gradient (10, 20, 30%) for 24hr each and then snap frozen in OCT prior to sectioning at 16 μm thickness. Fixed sections were baked at 60°C for 1 hr, washed with ethanol, followed by tissue pretreatment, probe hybridization following the RNAscope fluorescence multiplex assay and sections were counterstained with DAPI to visualize nuclei. Positive stained cells were identified as punctate dots present in nucleus and cytoplasm. Confocal Z stack images (every 0.2 μm) within the corpus callosum were taken (Zeiss LSM 510 Meta), and Z stacked images generated.

Animals and spinal cord surgery

All experiments were performed according to protocols approved by the University at Buffalo's Institutional Animal Care and Use Committee. Focal demyelination of adult (24 week) mouse spinal cord was induced as previously described (Zhao et al., 2006; Williver et al., 2018). Briefly, animals were anesthetized under isoflurane, and 0.5 μL 1% lysolecithin (Lα-lysophosphatidylcholine, Sigma) was directly injected into the dorsal and ventral funiculus of the spinal cord between two thoracolumbar vertebrae. For experiments involving IFN-γ, was diluted in 0.9% saline, mixed with 1% lysolecithin to a final concentration of 300U per injection and demyelination induced by injection of the mixture into the spinal cord. Animals were sacrificed at 5 days post-lesion (dpl) by transcardial

perfusion of saline followed by 4% paraformaldehyde under deep anesthesia. The spinal column was extracted, post-fixed for 30 min in 4% paraformaldehyde, the spinal cord isolated and processed as described above.

Statistical analysis

Statistical analyses were performed using Prism software (GraphPad Software). *In vitro* experiments were performed with at least three independent fetal samples, and differences among overexpression groups were compared using one-way repeated-measures ANOVA with Dunnett's multiple comparisons post-test. Differences among the groups for *in* vivo experiments were compared using one-way or two-way ANOVA with Bonferroni's or Dunnett's post-test where appropriate. Statistical significance was considered at $p < 0.05$. All data are reported as mean ± SEM.

Cell Reports, Volume *25*

Supplemental Information

Paired Related Homeobox Protein 1 Regulates Quiescence in Human Oligodendrocyte Progenitors

Jing Wang, Darpan Saraswat, Anjali K. Sinha, Jessie Polanco, Karen Dietz, Melanie A. O'Bara, Suyog U. Pol, Hani J. Shayya, and Fraser J. Sim

Supplemental Figures

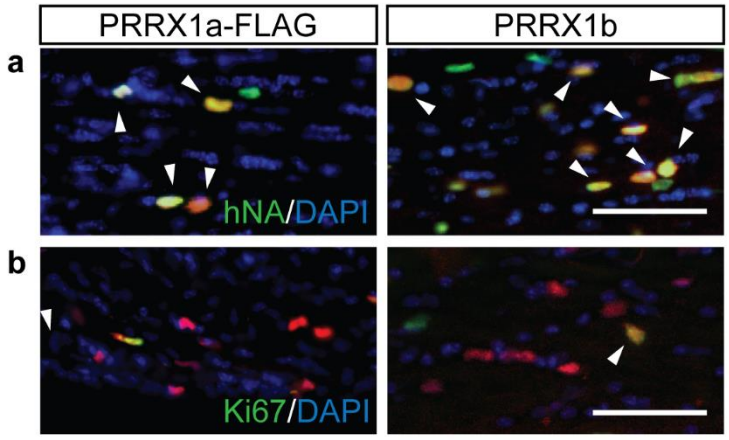

Figure S1 (related to Figure 3). PRRX1 over-expression was maintained for 12 weeks in engrafted human cells *in vivo*. Engrafted fetal human oligodendrocyte progenitors infected with PRRX1a or PRRX1b LV were examined after 12 weeks. **a,** PPRX1 expression was readily apparent in the majority of human (hNA; green) cells with antibodies recognizing the flag tag in the PRRX1a variant or specific to the PRRX1b variant (both in red). **b**, Proliferation of PRRX1 expressing engrafted cells was also confirmed by observing Ki67-PRRX1 double-positive cells. Arrowheads indicate double-positive cells. Scale: 50 µm.

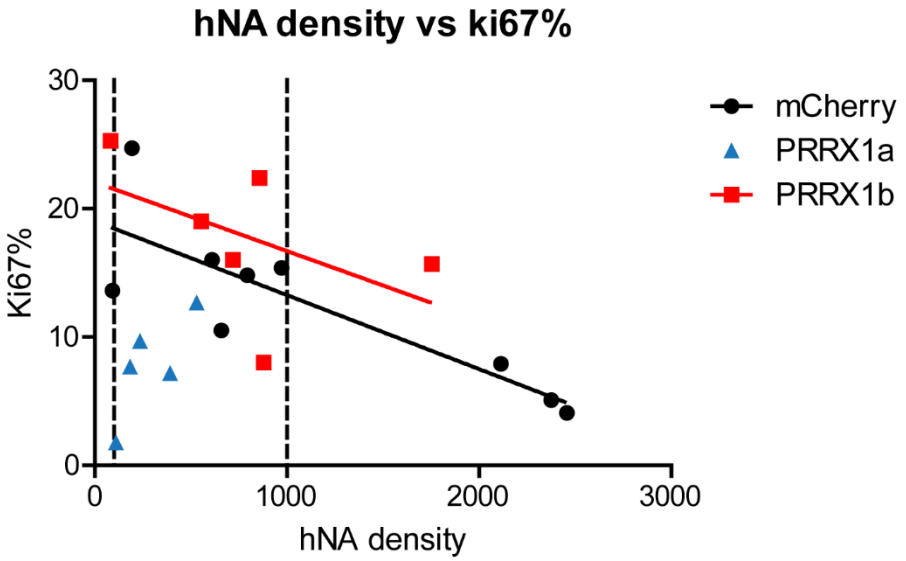

Figure S2 (related to Figure 3). Proliferation of human oligodendrocyte progenitors varies with density *in vivo*. Mice were sacrificed 12 wk following implantation of fetal human oligodendrocyte progenitors infected with a control mCherry lentivirus. Dashed lines demarcate range of densities used for Ki67 analysis. The density of implanted cells was calculated in regions within corpus callosum and plotted against the percentage of cells positive for Ki67 by immunohistochemistry ($n = 9$; $r^2 = 0.70$, $p < 0.01$, Pearson's correlation).

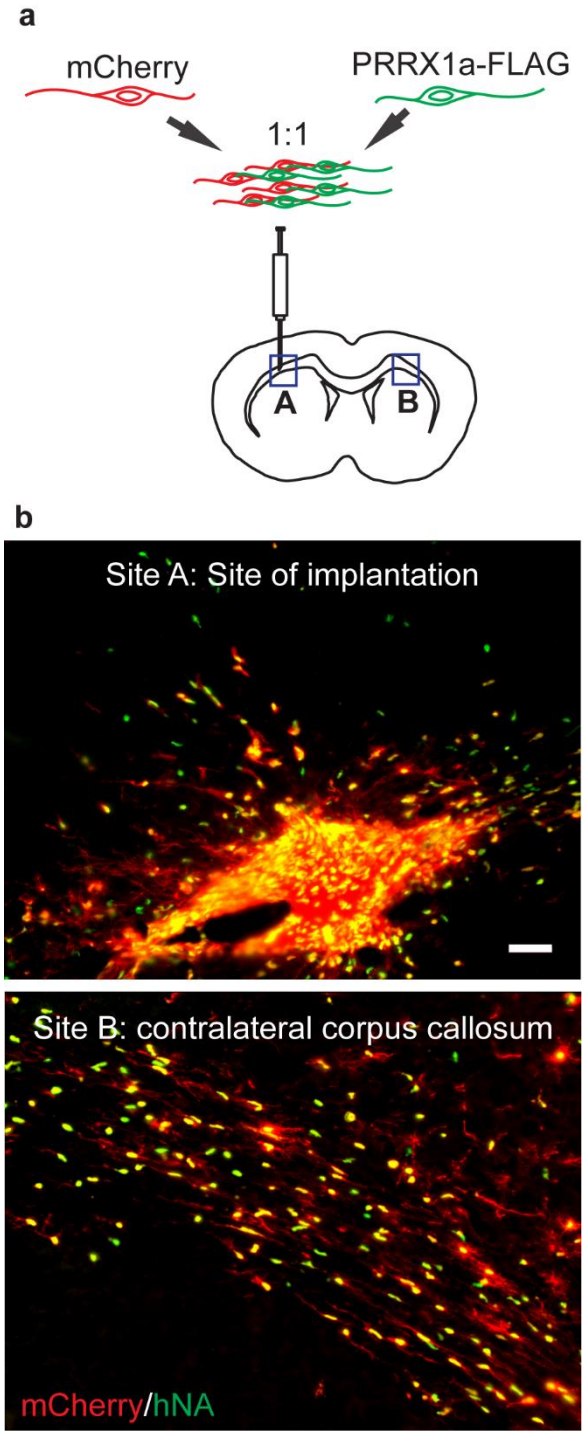

Figure S3 (related to Figure 3). Selective advantage of control hOPCs versus PRRX1-expressing quiescent hOPCs in *shiverer* forebrain. a, control mCherry-infected hOPCs were mixed 1:1 with PRRX1a-FLAG-infected hOPCs prior to unilateral engraftment into the corpus callosum of postnatal day 2-3 *shiverer/rag2* mice (n = 3). Mice were sacrificed at 4 wk to assess migration and engraftment of each population. **b**, the distribution of $mCherry^{+}hNA^{+}$ and $FLAG^{+}hNA^{+}$ cells was assessed at the site of implantation (A) and in the contralateral corpus callosum (B). The vast majority of hNA^{+} cells (green) co-expressed mCherry (red). In contrast to transplanted PRRX1a-$FLAG^{+}$ cells at 12 weeks (**Figure S1**), no $FLAG^{+}$ cells were detected at either site, indicating that PRRX1-infected hOPCs failed to successfully engraft. Scale: 50 µm.

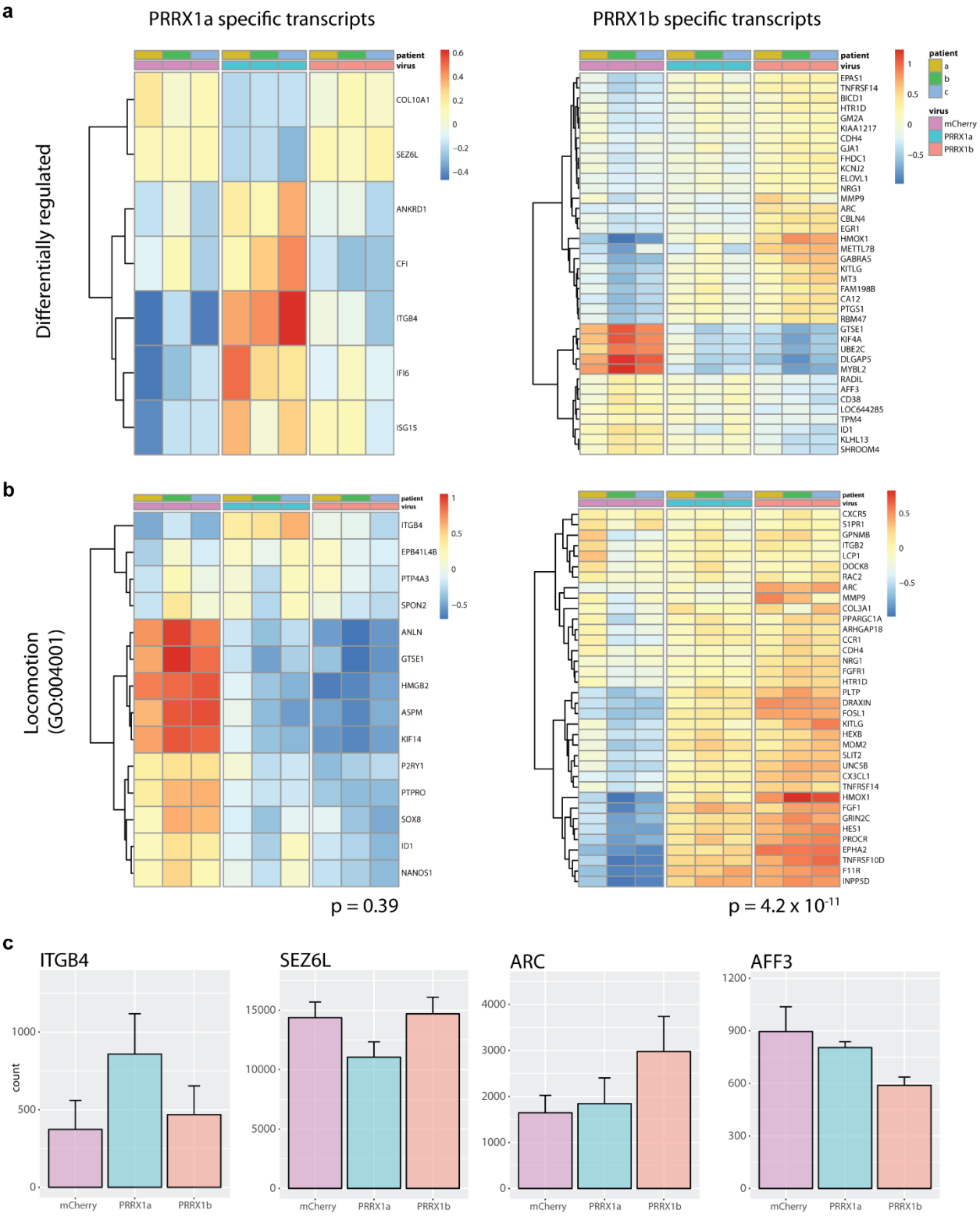
a
PRRX1a specific transcripts
PRRX1b specific transcripts
Differentially regulated
patient
virus
COL10A1
SEZ6L
ANKRD1
CFI
ITGB4
IFI6
ISG15
EPAS1
TNFRSF14
BICD1
HTR1D
GM2A
KIAA1217
CDH4
GJA1
FHDC1
KCNJ2
ELOVL1
NRG1
MMP9
ARC
CBLN4
EGR1
HMOX1
METTL7B
GABRA5
KITLG
MT3
FAM198B
CA12
PTGS1
RBM47
GTSE1
KIF4A
UBE2C
DLGAP5
MYBL2
RADIL
AFF3
CD38
LOC644285
TPM4
ID1
KLHL13
SHROOM4
a
b
c
mCherry
PRRX1a
PRRX1b
b
Locomotion
(GO:004001)
ITGB4
EPB41L4B
PTP4A3
SPON2
ANLN
GTSE1
HMGB2
ASPM
KIF14
P2RY1
PTPRO
SOX8
ID1
NANOS1
CXCR5
S1PR1
GPNMB
ITGB2
LCP1
DOCK8
RAC2
ARC
MMP9
COL3A1
PPARGC1A
ARHGAP18
CCR1
CDH4
NRG1
FGFR1
HTR1D
PLTP
DRAXIN
FOSL1
KITLG
HEXB
MDM2
SLIT2
UNC5B
CX3CL1
TNFRSF14
HMOX1
FGF1
GRIN2C
HES1
PROCR
EPHA2
TNFRSF10D
F11R
INPP5D
p = 0.39
p = 4.2 x 10-11
c
ITGB4
SEZ6L
ARC
AFF3
count
mCherry
PRRX1a
PRRX1b

Figure S4 (related for Figure 5). Analysis of splice-specific effects of PRRX1 over-expression on hOPCs. To better identify transcripts regulated by PRRX1 in a splice-specific manner, we used a modified linear model in which PRRX1 transcript level was used as an additional covariate. The PRRX1a and PRRX1b-infected hOPC transcriptomes were then compared by *edgeR* analysis and pathway analysis. **a,** Differential expressed transcripts between PRRX1a and PRRX1b ($q < 0.1$) were further filtered to include only those regulated significantly vs. mCherry-infected OPCs ($q < 0.05$). 7 genes were specifically regulated by PRRX1a and 38 genes by PRRX1b. Heatmaps show relative expression of *vst* normalized counts for each gene to the median level across samples (log2 scale shown). **b**, *topGO* analysis of transcripts regulated between 1a and 1b ($q < 0.1$) revealed that locomotion (GO:004001) were among the top 5 pathways up-regulated by 1b ($p = 4.2 \times 10^{-11}$). **c**, selected genes plotted based on normalized counts (pseudocount of 0.5; mean ± SEM, n = 3). All genes were significantly regulated between PRRX1a and PRRX1b conditions.

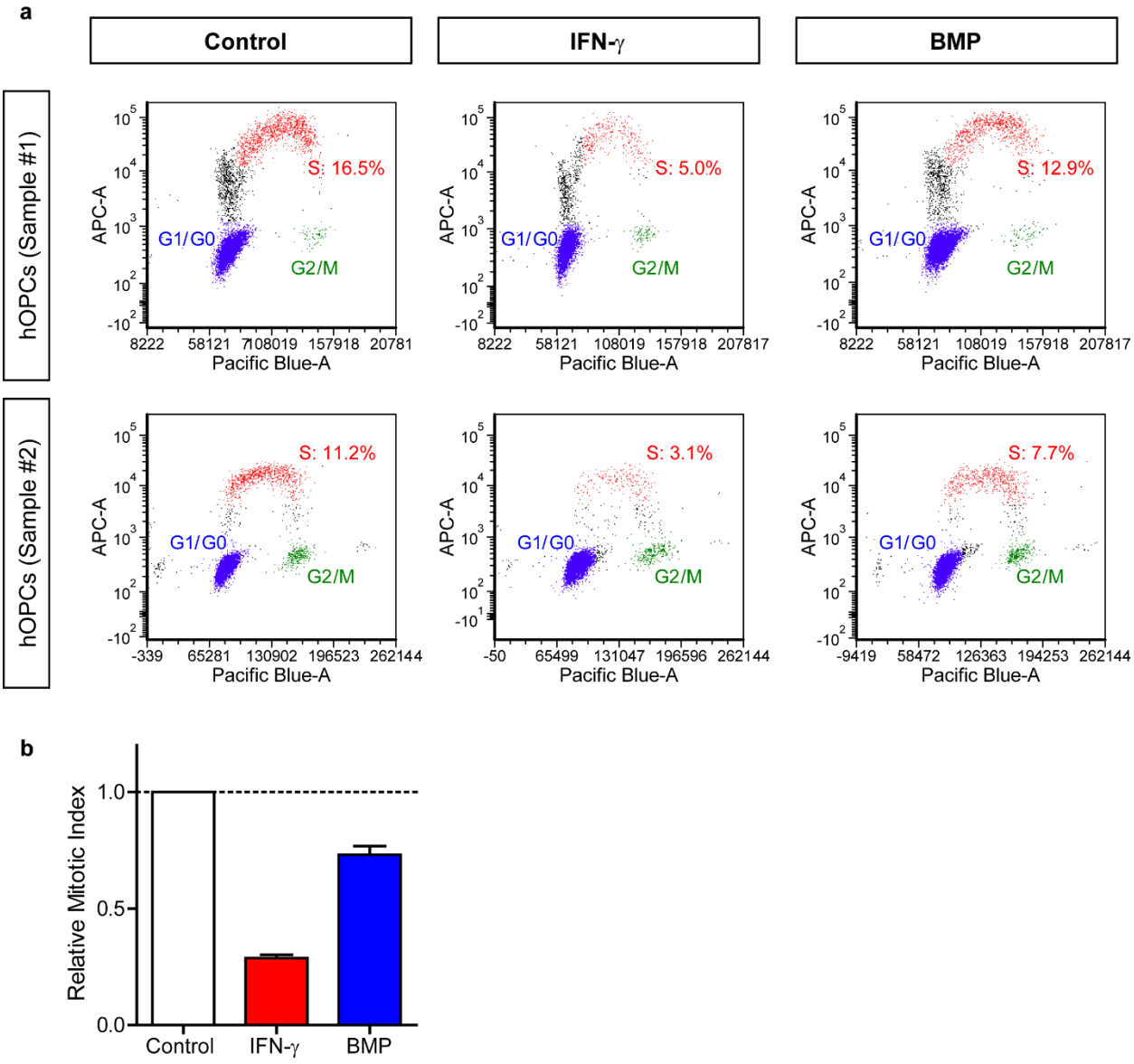

Figure S5 (related to Figure 6). IFN-γ and BMP reduce hOPC proliferation. a, hOPCs were grown in SFM without PDGF-AA (Control) or following addition of IFN-γ (10 ng/ml) or BMP-7 (50 ng/ml) for 24 hrs. Flow cytometry of S phase entry (red; 2-h EdU incorporation) and $G_{1/0}$ and $G_{2/M}$ phases (blue and green, respectively). Both IFN-γ and BMP7 treatment substantially reduced the proportion of S-phase hOPCs. The same number of events are shown in each dot plot following gating for singlet discrimination. **b**, quantification of mitotic index (defined as % S-phase relative to control cells) (mean ± SEM, n = 2 fetal human samples).

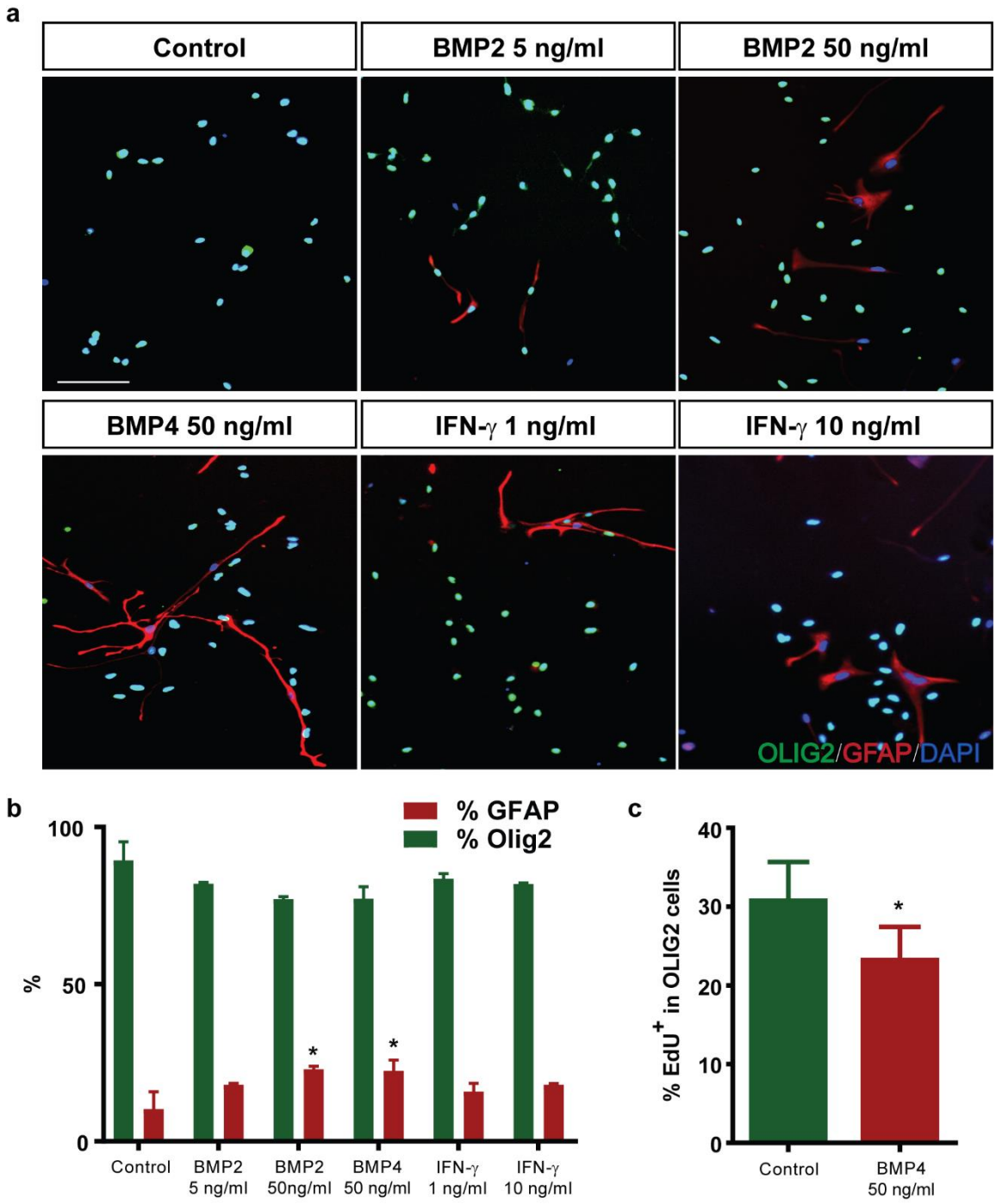

Figure S6 (related to Figure 6). Effect of BMP2/4 and IFN-γ on hOPC lineage and astrocyte differentiation. a, hOPC were treated with BMP2 (5-50 ng/ml), BMP4 (50ng/ml), or IFN-□ (1-10 ng/ml) for 24 hours. The effect of cytokine treatment on oligodendrocyte lineage commitment (OLIG2, green) and astrocyte fate (GFAP, red) was assessed by immunocytochemistry. **b**, Quantification of OLIG2+ and GFAP+ cells among DAPI+ cells (mean ± SEM, n = 3 fetal human samples, *p < 0.05, one-way ANOVA, Dunnett's multiple comparisons post-test vs. control). **c**, Proliferation of $OLIG2^{+}$ cells was assessed following terminal 8-hr EdU incorporation at 24 hours of BMP treatment. BMP4 (50 ng/ml) treatment caused a significant decrease in OLIG2+ cell proliferation relative to controls (paired t-test, $p < 0.05$, n = 3 fetal human samples). Scale: 50 µm.

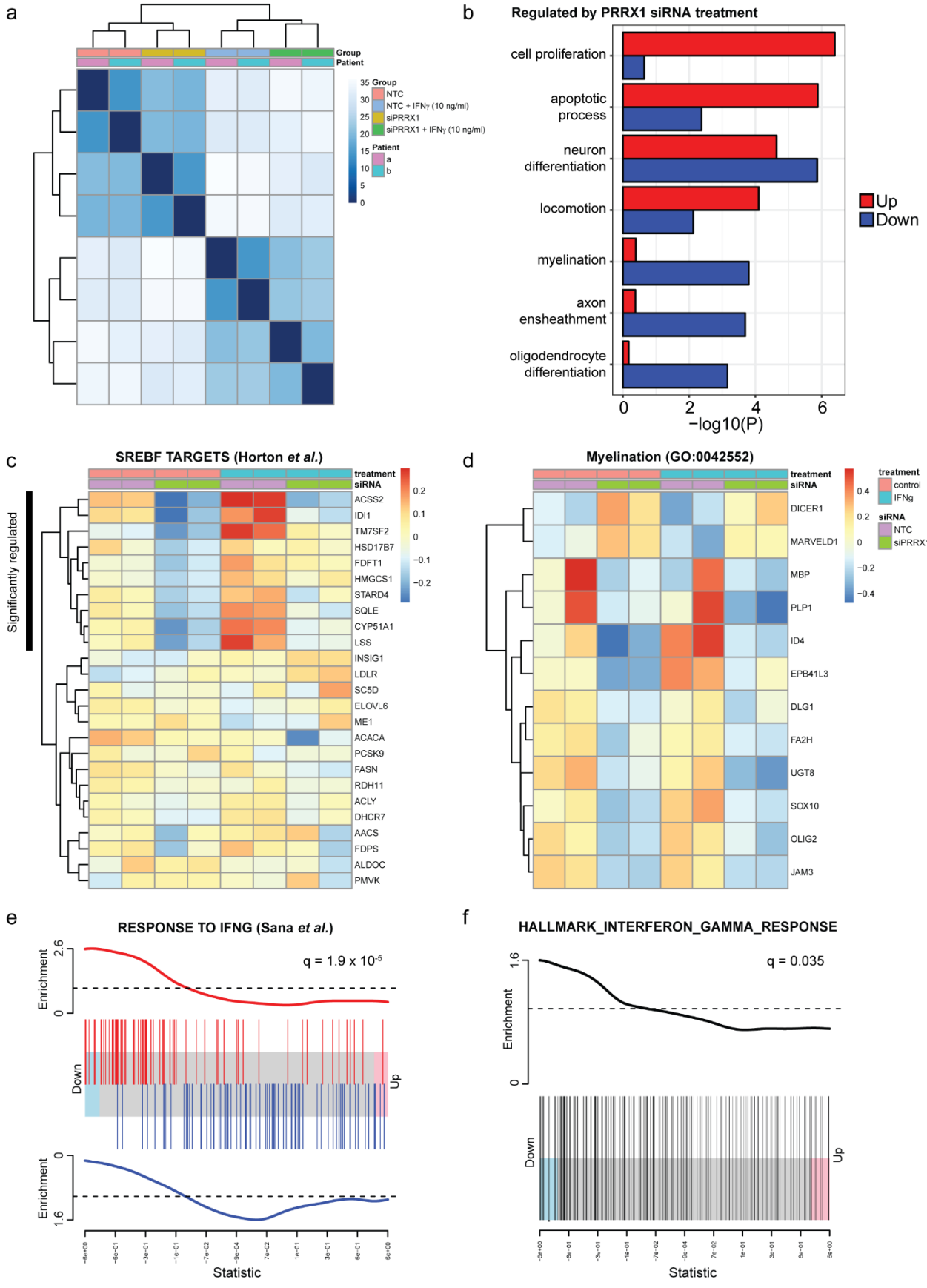
a
Group
Patient
35 Group
NTC
NTC + IFNγ (10 ng/ml)
siPRRX1
siPRRX1 + IFNγ (10 ng/ml)
Patient
a
b
b
Regulated by PRRX1 siRNA treatment
cell proliferation
apoptotic process
neuron differentiation
locomotion
myelination
axon ensheathment
oligodendrocyte differentiation
Up
Down
−log10(P)
c
SREBF TARGETS (Horton et al.)
Significantly regulated
treatment
siRNA
ACSS2
IDI1
TM7SF2
HSD17B7
FDFT1
HMGCS1
STARD4
SQLE
CYP51A1
LSS
INSIG1
LDLR
SC5D
ELOVL6
ME1
ACACA
PCSK9
FASN
RDH11
ACLY
DHCR7
AACS
FDPS
ALDOC
PMVK
d
Myelination (GO:0042552)
treatment
siRNA
DICER1
MARVELD1
MBP
PLP1
ID4
EPB41L3
DLG1
FA2H
UGT8
SOX10
OLIG2
JAM3
control
IFNg
NTC
siPRRX1
e
RESPONSE TO IFNG (Sana et al.)
q = 1.9 x 10-5
Enrichment
Down
Up
Statistic
f
HALLMARK_INTERFERON_GAMMA_RESPONSE
q = 0.035
Enrichment
Down
Up
Statistic

Figure S7 (related to Figure 6). PRRX1 siRNA reduces cholesterol biosynthesis and reverses IFN-γ induced gene expression. Human hOPCs were treated with IFN-γ (10 ng/ml) at 8 hrs post transfection and RNA extracted 24hrs later. **a**, Heatmap demonstrating clustering of individual RNA samples by sample-to-sample distances. The effects of IFN-γ and PRRX1 siRNA treatment on hOPC transcriptome are clearly distinguishable. **b**, Gene Ontology-based over-representation analysis of genes regulated by PRRX1 siRNA in hOPCs. **c-d,** Pathway analysis by gene set enrichment and topGO revealed PRRX1 target gene regulation of cholesterol biosynthesis genes (**c**, *camera* q = 0.0059) and myelination-associated transcripts (**d**, *topGO* $p = 1.6 \times 10^{-4}$). **e-f**, Gene set enrichment analysis examining the effect of PRRX1 siRNA on the IFN-γ induced transcriptional response demonstrated that PRRX1 siRNA was able to attenuate the induction of IFN-related transcripts. Red bars indicate the position of up-regulated genes and blue bars down-regulated genes in each gene set. The red/blue traces *above/below* show relative enrichment of up and down-regulated genes respectively (q-value shown).

Supplemental Tables

Gene / Target sequence	Sequence (5' to 3')
PRRX1a	Fwd: CGCAGGAATGAGAGAGCCAT Rev: AACATCTTGGGAGGGACGAG
PRRX1b	Fwd: ACGCTTCCCTCCTCAAATCC Rev: AGTAGCCATGGCGCTGTACG
CCNA1	Fwd: TTCCCGCAATCATGTACCCTG Rev: TGTAGCCAGCACAACTCCACT
CCNB1	Fwd: CGCCTGAGCCTATTTTGGTTG Rev: AGTGACTTCCCGACCCAGTA
CCNE2	Fwd: TCTTCACTGCAAGCACCATC Rev: ACCTCATTATTCATTGCTTCCAA
SGOL1	Fwd: GACCCCAATAGTGATGACAGC Rev: GAAATGATTCTCCTTGTCCTGG
RRM2	Fwd: CGGAGCCGAAAACTAAAGCAG Rev: TCTCCTCGGGTTTCAGGGAT
ANLN	Fwd: GCTGCGTAGCTTACAGACTTAGC Rev: AAGGCGTTTAAAGGTGATAGGTG
IRF1	Fwd: CAACATGCCCATCACTCGGA Rev: TGCTTTGTATCGGCCTGTGT

Table S1 (related to Figures 5 & 6). qPCR primers and Taqman assays used in this study.